

Progress Report No. 12

HYPERVELOCITY KILL MECHANISMS PROGRAM ARPA ORDER 149

Quarterly Technical Progress Report
For Period Ending
30 June 1963

**ADVANCED RESEARCH PROJECTS AGENCY
BALLISTIC MISSILE DEFENSE SYSTEMS BRANCH**

August 1963



**U. S. NAVAL RESEARCH LABORATORY
Washington, D.C.**

**APPROVED FOR PUBLIC
RELEASE - DISTRIBUTION
UNLIMITED**

CONTRIBUTORS

Aeronautical Research Associates of Princeton
AVCO Mfg. Co. - RAD Division
Ballistic Research Laboratories
General Electric Co. - MSD
Naval Research Laboratory

This document contains information affecting the national defense of the United States within the meaning of the Espionage Laws, Title 18, U.S.C., Sections 793 and 794. The transmission or revelation of its contents in any manner to an unauthorized person is prohibited by law.

Further distribution of this report or of an abstract or reproduction may be made only with the approval of the Director, U.S. Naval Research Laboratory, Washington 25, D.C. or of the activity sponsoring the research reported therein as appropriate.

CONTENTS

	Page Designation
Problem Status	ii
Authorization	ii
INTRODUCTION	1
HKM PROGRESS REPORTS	
I. IMPACT DAMAGE PHASE	
Ballistic Research Laboratories	A
U.S. Naval Research Laboratory	
Section I	B
Section II	B'
II. AEROTHERMAL PHASE	
AVCO Mfg. Company - RAD	C
General Electric Company	H
Aeronautical Research Associates of Princeton	L
III. DISTRIBUTION	Z

i
APPROVED FOR PUBLIC
RELEASE - DISTRIBUTION
UNLIMITED

PROBLEM STATUS

This is a quarterly letter progress report covering the work of the participants in the Hypervelocity Kill Mechanisms Program; work on this problem is continuing.

AUTHORIZATION

NRL Problem No. F04-11
ARPA Order No. 149-60

INTRODUCTION

Progress Report No.12 is a compilation of quarterly technical progress reports covering the work of the Hypervelocity Kill Mechanisms Program for the period covering 20 March through 30 June 1963.

The reports cover the work performed in the impact damage and the aerothermal phases of the Program. The work covering the impact damage and aerothermal phases was done by the Aeronautical Research Associates of Princeton, AVCO-RAD, Ballistic Research Laboratories, U.S. Naval Research Laboratory, and General Electric Company.

B A L L I S T I C R E S E A R C H L A B O R A T O R I E S

HYPERVERLOCITY KILL MECHANISMS PROGRAM

ARPA Order 149-60

IMPACT DAMAGE PHASE

Quarterly Progress Report
For Period Ending
20 June 1963

A. Pillersdorf
S. Kronman

A B E R D E E N P R O V I N G G R O U N D , M A R Y L A N D

SUMMARY

Investigation of composite target combinations (non-metallic face-plate plus metallic back-up) was continued in three additional phases (III-V inclusive) with one observation per condition. The target combinations (1" face-plate + 1/8" back-up at 30-degree attack angle, 2" + 1/8" at normal incidence, and 1" + 1/4" at normal incidence) were attacked by aluminum inhibited jet pellets with the same impact characteristics provided in the previously reported tests. The target hole dimension data obtained were used as a basis for evaluation of the effects of attack angle and additional face-plate and back-up plate thickness combinations under the same impact conditions of the previous tests.

Thin plate perforation studies were completed using steel equi-axed cylinders in the velocity range of 2 to 5 km/sec. Characteristics of the mass, velocity, and spatial distribution of rear surface ejecta were determined as the impact velocity, projectile size and target thickness were varied. For the case of the non-deforming projectile, it was shown that residual projectile velocity and target impulse can be predicted on the basis of a simple mathematical model. Most recently, the thin plate penetration studies were extended to include experiments with much higher velocity projectiles provided by an inhibited jet design developed at BRL. Impacts on aluminum, magnesium, and steel targets observed thus far are incorporated in summaries of target reactions.

COMPOSITE TARGETS

In Phase III, four one-inch face targets - glass, fiberglass laminate, phenolic nylon laminate, and polyethylene, each with three different one-eighth inch back-ups - aluminum, magnesium, and steel - were attacked at thirty degrees (60-degree obliquity).

Throat hole dimensions of the face-plate materials showed no tendency to differ from those obtained at normal incidence at all thickness combinations. The back-up plate hole dimensions at the thirty degree attack angle tend more toward those of back-up plates in combinations of equal thickness than toward those in combinations of equivalent thickness (2" + 1/4"). The effect of rolling direction of the metallic back-up plates on the non-circular hole dimensions appears to be more pronounced in some instances of this oblique attack phase.

In Phase IV, the face-plate thickness was changed to two inches while the back-up plate thickness remained at 1/8th inch. The attack angle was ninety degrees. Of the twelve original target combinations, the three with glass face plates were omitted. A comparison of results with those of Phase I against two-inch face-plates with quarter-inch back-ups does not show a tendency of primary-target-throat-hole diameters to vary with changes in back-up thickness. The back-up hole dimensions in nearly all cases increase with thinner back-up plates.

For Phase V, glass combinations were again excluded and the thickness pairings were reversed to one-inch face with quarter-inch back-ups. Attack conditions were the same as in Phase IV. By comparison with Phase II, 1/8th inch back-ups, the tendency for back-up hole dimensions to increase with decreased back-up thickness was even more pronounced than for the preceding Phase IV. As in Phase IV, there is no marked tendency of primary-target hole-diameters to vary with back-up thickness.

For the impact condition and target combinations used to date, there appears to be a tendency for the hole dimensions of both the 1/8 and 1/4 inch metallic back-up plates to increase with an increase in primary plate thickness from one to two inches. This tendency appears more pronounced for the quarter-inch, especially the aluminum plates. The hole dimensions of all three back-up plates, however, are consistently smaller in the combinations of greater thicknesses (2" + 1/4") than in those of the lesser thicknesses (1" + 1/8").

Further clarification of shock-distribution and attenuation processes is expected from the shock-pulse measurement program. The composite target program will be continued with the original four face-plate and three metallic back-up materials, but with an attacking pellet of approximately eight times the present mass.

THIN PLATE STUDIES

Research on impact damage to thin and thick 2024-T3 aluminum targets was continued with two basic explosive projector systems. One system utilized a 0.02 gram steel projectile, the other a 0.187 gram projectile. While velocity levels of 2.0, 3.2 and 4.0 km/sec were used for the lighter projectile, the velocity of the heavier projectile was increased to 5.0 km/sec by use of a BRL air-cavity projector. The pertinent variables studied for thick targets were crater depth, diameter and volume; for thin targets, entrance and exit diameters.

For thick targets, crater volume was found proportional to the kinetic energy of the projectile. At low impact velocities, the craters are narrow and deep, while at velocities approaching the sonic velocity of the target material (5.1 km/sec) the craters approach a hemispherical shape.

For thin targets (of thickness exceeding 1.5 times the projectile length) the perforation entrance diameter is independent of target thickness. For targets of lesser thickness, a decrease in entrance diameter was noted.

The spall particle distributions produced by projectile-target impacts over the 2-5 km/sec range were analyzed from a spatial distribution standpoint for both normal and oblique incidence. Consistent with previous indications, the percentage of the total number of spall fragments in a given space element was found independent of projectile scale size, projectile velocity, or target thickness. In the case of oblique impacts, spall particle distribution characteristics are complicated by a dependence on azimuthal angle (lateral angle relative to line of flight) and cannot be described in as simple terms as hold for the normal impact case. The center of spall impact is displaced radially outward along zero azimuth, the direction of the line of flight of the projectile.

An analysis of the manner in which the mass contained in the spall envelope is distributed spatially shows qualitative similarities to the particle number distributions derived previously for normal incidence, from which the inference is drawn that spall particle size is not particularly dependent upon the space coordinates.

By use of a flash x-ray system for determining residual projectile velocity and a ballistic pendulum for target impulse studies, values of total target-spall momentum have been obtained. Photographic determination of average exit velocities of spall and projectile particles has led to further applicability of a particle residual velocity formula developed in earlier studies.

The photographic determination of the velocity distribution of individual ejecta particles indicates that, for scaled systems, the velocity distributions are similar in that both the maximum spall velocity and the velocity of the maximum percentage of the total number nearly coincide.

Analysis of results has also shown that, for the non-deforming projectile, the residual projectile velocity and target impulse can be predicted on the basis of a simple mathematical model.

Most recently, the thin target studies were extended to include experiments featuring projectiles of the BRL inhibited-jet type at impact velocities of 9.5 km/sec. Limited data obtained for spall systems with aluminum, magnesium and steel targets indicate:

The distributions for spall numbers and masses are similar to those obtained with the lower velocity projectiles, i. e. , maximum density occurs at the center of impact and diminishes radially outward. Spall particle size continues to increase markedly with increase in target thickness. The target perforation and spall diameters vary with thickness and material in a manner qualitatively similar to results obtained with 5 km/sec projectiles.

Studies with the 9.5 km/sec inhibited jet projectile are being continued with several target materials for extension of previously derived target and spall momentum relationships.

QUARTERLY TECHNICAL PROGRESS REPORT NO 12
FOR PERIOD ENDING
30 JUNE 1963

SECTION I
IMPACT DAMAGE

J.J. Condon
S.M. Halperson

SECTION II
IMPACT DAMAGE BY LARGE MASS MATERIALS

C.D. Porter
J. Davis

This Research Was Supported By the Advanced
Research Projects Agency, Ballistic Missile
Defense Systems Branch.

Dynamics Branch
Mechanics Division

U.S. NAVAL RESEARCH LABORATORY
WASHINGTON, D.C.

CONTENTS

	<u>Page No.</u>
PROBLEM STATUS	ii
AUTHORIZATION	ii
LIST OF FIGURES	iii
SECTION I. IMPACT DAMAGE	B
Summary	B1
Introduction	B2
Progress	B2
Astrolite	B3
Phenolic Nylon	B3
GE Series 124A	B5
Conclusions and Future Plans	B6
Table I - Hole Dimensions For Previously Reported NRL Data	B8
Table II - Impact Characteristics	B9
PROBLEM STATUS	B'i
AUTHORIZATION	B'i
LIST OF FIGURES	B'ii
SECTION II - IMPACT DAMAGE BY LARGE MASS MATERIALS	B'
Summary	B'1
Introduction	B'2
Impact Analysis	B'2
Optical	B'2
Structural Analysis	B'3
Accelerator Techniques Development	B'4
Large Gun Prototype	B'4
Ring Seal Sabot Development	B'5
Hydraulic Piston	B'5
Petal Valve	B'5
Future Work	B'6
Instrumentation	B'6
Density Effect	B'7
REFERENCES	B'8

PROBLEM STATUS - SECTION I

This is a Quarterly Technical Progress Report.
Work on this Project is Continuing.

AUTHORIZATION

NRL Problem 62F04-11B

ARPA Order No. 149-60

Amendments 1 - 7

LIST OF FIGURES

FIGURE

1. Hole Size vs Impact Energy per Unit of Ablative Thickness For Phenolic Refrasil
- 2a. Round No. 4-865, 12" x 12" x 1" Laminated Astrolite with a 0.25" Al Back-up Impacted at 90° with a 5/16" Steel Sphere (2.04 gm) at a Velocity of 5.037 km/sec.
- 2b. Round No. 4-866, 12" x 12" x 1" Random Chopped Squares Astrolite with a 0.25" Al Back-up Impacted at 90° with a 5/16" Steel Sphere (2.04 gm) at a Velocity of 4.970 km/sec
- 3a. Round No. 4-851, 12" x 12" x 1" Random Chopped Squares Phenolic Nylon with a 0.25" Mg Back-up Impacted at 90° with a 1/4" Steel Sphere (1.045 gm) at a Velocity of 4.75 km/sec
- 3b. Round No. 4-852, 12" x 12" x 1" Random Chopped Squares Phenolic Nylon with a 0.25" Mg Back-up Impacted at 90° with a 1/4" Steel Sphere (1.045 gm) at a Velocity of 4.75 km/sec
- 3c. Round Nos. 4-851 and 4-852, Recovered Front Spall Pieces Placed Back Into Spall Cavity After Impact
- 3d. Round Nos. 4-851 and 4-852, 0.25"-thick Aluminum Witness Plates placed 10" behind Target
- 4a. Round No. 4-871, 12" x 12" x 1" Laminated Phenolic Nylon with a 0.25" Al Back-up Impacted at 90° with a 5/16" Steel Sphere (2.04 gm) at a Velocity of 5.0 km/sec
- 4b. Round No. 4-867, 12" x 12" x 1" Random Chopped Squares Phenolic Nylon with a 0.25" Mg Back-up Impacted at 90° with a 5/16" Steel Sphere (2.04 gm) at a Velocity of 4.54 km/sec
5. Hole Size vs Impact Energy per Unit of Ablative Thickness for Phenolic Nylon
6. Hole Size vs Impact Energy per Unit of Ablative Thickness for GE 124A.

SUMMARY

Perforation of composite targets with spherical projectiles of known mass and velocity fired at different angles was emphasized. In order to better establish correlations of the impact effects on various ablative materials and to analyze the results, both velocity and energy range of the projectiles were varied. Approximately 45 experiments were conducted, with sabotaged steel and nylon spheres having velocities between 3-6 km/sec. The materials impacted were laminated and random-chopped phenolic refrasil and nylon and G.E. Series 124A. Back-up materials were 1/4-inch thickness aluminum and magnesium for the phenolics and 1-inch aluminum honeycomb for the 124A. Correlations of the hole size with target thickness and composition, projectile energy, velocity, size and density were examined for each of the composite targets.

INTRODUCTION

The purpose of the work presented is to determine the impact effects on ablative materials and re-entry vehicle structures from hypervelocity impact with compact projectiles of various densities, for example; aluminum, steel and uranium. Analytical means will be used to explain the experimental results and to correlate significant parameters so that accurate and reliable impact predictions can be made. These data provide part of the information needed for determining the feasibility of defeating an enemy ICBM by fragment impact.

PROGRESS

The impact experiments for this quarter are summarized in Table II. Table I is a list of hole areas and equivalent perforation diameters with the corresponding Round Nos. for data previously reported in progress reports No. 9 and 11. The projectiles were sabot steel and nylon spheres. The composite targets were GE 124A and phenolic refrasil and phenolic nylon bonded to 0.25-inch aluminum. The impact results and the correlations that have been obtained for each material are discussed separately. Figures 1, 5, 6, 7 show the best correlations that have been obtained at this time. In the next annual report curves will be fitted to the best data correlations that exist at that time so that the impact results for different materials can be compared. In these figures Round Nos. are written above each data point. With this identification number and referring to Tables I and II in this report and similar tables in progress reports No. 9 and 11 all the conditions under which the data were obtained can be determined.

Astrolite

The laminated and random-chopped refrasil phenolic materials that were impacted this quarter are listed in Table II. The back-up material was 0.25-inch aluminum. The projectiles were primarily 1 and 2-gram steel spheres with velocities ranging from 3 to 5.8 km/sec. Figure 1 is a graph of the equivalent hole diameter D_a in the ablative vs impact energy per unit of ablative thickness for all the astrolite data that has been obtained at NRL. The laminated and random-chopped molded types are designated by triangles (Δ) and circles (O) respectively. The data shown represent a wide

range of conditions. The ablative thicknesses were varied from 1/2 to 2-inches. The back-up materials were primarily aluminum with some steel. Back-up thicknesses varied up to 0.25-inch. The projectiles were steel, aluminum and plastic (Lexan) spheres and cylinders. All projectiles except the plastic were sabotaged. Impact angles varied from 90° (normal impact) to 15°. Projectile velocities covered a range from approximately 3 to 7 km/sec; masses from 1 to 15 gm. This corresponds to impact energies of 10 to 350 Kj. Considering this wide range of impact conditions the correlation appears good. A least squares curve will be fitted to this data or improvements of it in the next report.

No consistent difference can be seen in the perforation diameters for the laminated and random-chopped types of Astrolite. However there is a difference in the front spall characteristics of the two types. As shown in Figure 2 the front spall area in the laminated material is not much larger than the perforation area. In contrast to this, the spall area of the random-chopped astrolite is substantially larger than the perforation area. The similarities and differences in the spall characteristics for the astrolite and phenolic nylon are pointed out in the discussion of the impact results of the phenolic nylon.

In the impact experiments with the phenolic refrasil material the back-ups usually came off the back of the ablative material during the impact. This material was procured without back-ups. Bonding was done in-house with a very thin bond of glue. In contrast to this, the back-ups stayed on the ablative materials that were received with the back-ups bonded to the ablative material by the manufacturer with a type of rubbery bond. These bonds were approximately 1/16-inch thick.

Phenolic Nylon

The impact results for the phenolic nylon material obtained during this quarter are listed in Table II. The targets were laminated and random-chopped phenolic nylon with 0.25-inch thick aluminum and magnesium back-ups. The velocities for the 1 and 2 gm. steel spheres were varied between 3 and 5 km/sec in order to establish a basis for correlation. The changes in the impact results are more erratic than for the astrolite material, causing considerable difficulty in the analysis of results. An example of this inconsistency is

shown by the results from Rounds 4-851 and 4-852, see Table II, and Figure 3. These two targets appeared to be the same in all respects. Impacts were made with a 1/4-inch steel sphere at approximately 15,500 ft/sec. As can be seen in Figure 3 the hole diameters are very different. There is no quantitative explanation of these results at this time. These differences may be due partly to the inhomogeneous nature of the material and the orientation of the random-chopped squares. It is felt that these erratic results will diminish as the velocity and energy levels are increased.

Another difference that has been observed between the laminated and random-chopped squares is the shape of the front spall cavity. For the random-molded phenolic nylon the depth of the spall cavity varies in a gradually increasing amount from the outside of the spall cavity toward the center of the perforation. The type of spall cavity left after impact into the laminated material is more sharply defined. The depth of the cavity is more nearly constant from the outside of cavity toward the center where the perforation is located, see Figure 4. These spall characteristics for the random-chopped phenolic nylon are very similar to the random chopped astrolite. The type of spall produced in the laminated astrolite is different than the spall cavity left in the laminated phenolic nylon. An example of this can be seen by comparing Figure 2a with Figure 4a.

The recovered front spall pieces that are shown in Figure 3c are often observed from low energy impacts into the random-chopped materials. The resulting shock-wave intensities from impact are not large enough to completely disintegrate the front spall pieces but are intense enough to fracture the material around the perforation and loosen large pieces of spall. The small hole where the projectile entered the material is clearly discernible.

A correlation of the equivalent perforation diameter in the ablative vs energy per unit thickness of the ablative for all the phenolic nylon data is shown in Figure 5. Further work is necessary in order to make the results more definitive. Although various modifications to this correlation have been tried e.g. normalizing the hole diameter or hole area, none have been successful. Other correlations such as hole diameter vs impact velocity have not yet resulted in anything significantly better.

GE Series 124A

A summary of the impacts into the 124A material with nylon and steel spheres is shown in Table II. The 1/4" diameter nylon sphere (0.1560 gm) impacting at 90°, did not perforate the composite target for velocities up to 6.58 km/sec (rounds 5-3-60 to 5-3-67). The 7/16" ablative material was perforated at a velocity of about 4.6 km/sec (see round number 5-3-64). The projectile was still visible in the bottom of the crater after impact in round numbers 5-3-60, 61, 62. The projectile was removed from the bottom of the crater in the ablative material for round number 5-3-62 and the weight of the nylon sphere was about the same as before impact. It could be seen from visual inspection that part of the projectile was composed of ablative material fused to the original nylon. Although the nylon sphere did not perforate the back-up, the associated impact in rounds 5-3-66, 67 did loosen the last aluminum plate in the honeycomb sandwich from the honeycomb for more than half the surface of contact.

Correlations of the projectile parameters and the impact results on this material are not complete; however comparison of the equivalent hole diameter in the ablative vs impact energy per ablative thickness is shown in Figure 6 for all the steel sphere impacts. The results show that the impact effects for this material are more dependent on the impact angle than are the phenolic materials. It was pointed out in Progress Report No. 11 that for the data obtained up to that time the angle of impact did not make a large difference in the diameter of the perforation as long as the energies were above the minimum perforation value. This is still true for the phenolic materials but not for the 124A material. In this material both minimum perforation and the hole diameter are dependent on the angle of impact. Qualitatively this can be regarded as a tendency for the projectile to glance along the surface of the material, which would tend to increase the impact area and increase the hole size, especially if the material is brittle like 124A. An example of this smearing out of the area of impact is shown in Progress Report No. 11, Figure 9, for a 30° impact into plexiglas. Some size effect depending on the angle of impact will have to be used to correlate this data for impacts which are not 90°.

Figure 7 is a comparison of the equivalent hole diameter in the ablative material vs impact velocity for 90° impacts with 1/4" steel and nylon spheres. Round Numbers 1-2-9 to 1-2-18 were impacts of this material with 1/4-inch steel spheres at velocities from 3.86 to 5.57 km/sec. The steel spheres completely perforated the target at all of the velocities in this range.

Although the penetration characteristics of the steel and nylon spheres are considerably different it can be seen that the resulting hole size in the ablative using these two types of projectiles is similar when compared at the same velocity. This result is also shown by the impact data on the phenolic refrasil materials with steel back-ups. (see Figure 1 round nos. 1-1-32 and 1-1-65). The hole size using these two plastic (Lexan) cylinders is compared with the data for steel projectiles although the steel back-ups were not perforated in either case by the plastic cylinders.

CONCLUSIONS AND FUTURE PLANS

The best correlation that has been obtained for all three groups of materials is an impact energy/unit thickness of ablative vs hole size in the ablative. Other correlations which have been briefly examined have not been satisfactory. These were correlations of ablative perforation area, normalized ablative hole area and diameter vs projectile impact velocity, energy and momentum. The hole diameters in the 124A material are dependent on the angle of impact, increasing as the impact angle decreases. A correlation of impact velocity vs equivalent perforation diameter in the ablative was obtained for normal impacts (90°) with the 1/4" steel and nylon spheres. Various ways of accounting for the larger holes in the 124A material at impact angles of less than 90° were attempted, but were not satisfactory. In the annual report a least squares fit will be used on the data for each group of materials with the best correlations which have been obtained.

No consistent difference has been noted so far between the equivalent perforation diameters in the laminated and random-chopped squares phenolic materials. The front spall cavity is larger than the ablative hole diameter for the random-chopped astrolite and phenolic nylon, and the laminated phenolic nylon. In contrast to this there is not much of a front spall cavity in the laminated astrolite for most of the impact experiments.

Approximately 35 impact experiments are planned for the next quarter. The targets will be primarily Astrolite with steel back-ups. The projectiles will be aluminum, steel and uranium spheres and cylinders. The projectiles will have velocities of 6-7 km/sec and masses up to 10 grams. The emphasis will be to more clearly define the effects of projectile density, mass and velocity on the hole size in the ablative materials.

TABLE I - HOLE DIMENSIONS FOR PREVIOUSLY
REPORTED NRL DATA

Round No.	A_a cm ²	D_a cm
5-3-16	1.48	1.37
5-3-18	3.35	2.07
5-3-20	1.35	1.31
5-3-24	25.55	5.70
5-3-25	31.16	6.30
5-3-28	29.74	6.15
4-784	26.32	5.79
4-785	28.13	5.98
4-797		2.52
4-734		
5-3-4		
5-3-2		
5-3-7		
4-736		
4-421	6.23	2.82

TABLE II
IMPACT CHARACTERISTICS

Ablative Material Size	Back-up Thickness	Size	Material	PROJECTILE			ABLIATIVE MATERIAL				BACK-UP		Remarks	Round #	
				Impact Angle (Deg.)	Impact Velocity (ft/sec) (km/sec)	Normal Component of vel. (ft/sec) (km/sec)	Impact Energy & Energy Using Normal Vel. (kjoules)	Fenestration (cm)	Hole Dimensions (cm)	Minimum Dia (cm)	Area (cm ²)	Hole Diameter (cm)			Dimensions (cm)
12"X12"X1" Ast. L.	0.25" 2024 T3 Al	Sphere 1/4" Dia	Steel C65	90°	15,523 (4,731)	11,695	Complete Perf.	3.2	3.0	2.7	7.87	3.17	2.8	1.3	1-2-19
12"X12"X1" Ast. L.	"	"	"	90°	16,131 (4,916)	12,627	"	3.6	3.3	"	7.61	3.11	1.8	1.7	1-2-20
12"X12"X1" Ast. L.	"	"	"	90°	15,394 (4,692)	11,503	of abl. only	2.6	2.4	"	4.13	2.29	Back-up not perforated	"	1-2-21
12"X12"X1" Ast. L.	"	Sphere 5/16" Dia	"	90°	16,527 (5,037)	25,866	Complete Perf.	5.5	4.9	"	21.25	5.2	5.2	4.5	Small Sabot hit - Back-up separated, some delamination
12"X12"X1" Ast. L.	"	"	"	90°	14,719 (4,486)	20,514	"	4.2	4.1	"	15.81*	4.49*	5.2	4.25	Back-up separated, some delamination
12"X12"X1" Ast. L.	"	"	"	90°	10,731 (3,270)	10,907	"	3.3	3.0	"	9.0	3.38	3.6	2.6	Back-up separated
12"X12"X1" Ast. R.C.M.	"	"	"	90°	11,035 (3,363)	11,527	"	2.8	2.8	"	6.19	2.81	"	"	4-854
12"X12"X1" Ast. R.C.M.	"	"	"	90°	13,462 (4,103)	17,168	"	6.2	3.5	"	12.38	3.97	"	"	Sabot cap aggravated perforation
12"X8"X1" Ast. R.C.M.	"	"	"	90°	14,693 (4,478)	20,445	"	4.3	3.4	"	11.42	3.81	"	"	Target cracked slightly
12"X12"X1" Ast. R.C.M.	"	"	"	90°	16,308 (4,970)	25,190	"	5.2	3.5	"	14.45*	4.29*	6.8	6.7	Back-up separated
12"X12"X1" Ast. R.C.M.	"	"	"	90°	10,232 (3,118)	9,907	"	3.3	2.85	"	7.11	3.01	3.2	2.9	"
12"X12"X1" Ast. L.	"	Sphere 1/2" Dia, 2024-ST3	Al	90°	18,961 (5,779)	50,096	"	5.75	5.3	"	18.90	4.91	9.6	7.5	"
12"X14"X1" Ph.Ny.L.	"	Sphere 5/16" Dia, C65	Steel C65	90°	10,638 (3,242)	10,690	"	1.0	0.7	"	1.35	1.31	2.1	2.0	"
12"X12"X1" Ph.Ny.L.	"	"	"	90°	11,101 (3,384)	11,678	"	6.4	2.8	"	8.155	3.22	6.7	5.8	Sabot cap aggravated the perforation

*Thin lip partially covering perforation
Larger area used

TABLE II Con't
IMPACT CHARACTERISTICS

Ablative Material Size	Back-up Thickness	Sphere Size	Material	Mass (gm)	PROJECTILE			ABLATIVE MATERIAL				BACK-UP		
					Impact Angle (deg.)	Impact Vel (ft/sec)	Normal Component of vel. (ft/sec)	Impact Energy (kjoules)	Penetration (cm)	Hole Dimensions (cm)	Min-Dia (cm)	Area (cm ²)	Hole Dia (cm)	Dimensions (cm)
12"X12"X7/16" 124A	1" Honey-comb	Sphere 1/4"Dia	Steel C65	1.045	90°	14,674	10.454	Complete Perf.	3.7**3.7**	3.61	2.14	5.7	4.8	1-2-16
12"X12"X7/16" 124A	"	"	"	1.045	90°	17,269	14.506	"	3.8**3.8**	2.54	1.80	7.4	5.4	1-2-18
12"X10"X7/16" 124A	"	"	"	1.045	15°	17,295	14.525	See Remarks	5.56 3.82	3.22	16.52	4.59	Back-up not perforated for about 3 5/8"	5-3-58
12"X12"X7/16" 124A	"	"	"	1.045	90°	18,280	16.220	Complete Perf.	3.0 3.0	7.07	3.0	13.0	6.0	Sabot damage 1-2-14
12"X10"X7/16" 124A	"	Sphere 3/16"Dia	"	0.44	15°	17,315	6.117	2.64	1.94 0.99	0.73	1.42	1.34	Back-up not perforated on 2nd Al 5-3-54 plate	5-3-54
12"X24"X7/16" 124A	"	"	"	0.44	15°	18,420	6.927	2.80	2.11 1.10	0.75	1.94	1.57	5-3-57	
12"X12"X7/16" 124A	"	1/8"Dia	"	0.131	90°	13,517	1.108	Complete Perf.	0.5 0.5	0.32	0.64	0.7	0.6	5-3-51
12"X12"X7/16" 124A	"	"	"	0.131	15°	15,585	1.472	.066	Dimensions of indentation in ablative 1.03-0.38					Back-up not perforated 5-3-52

* Small piece of ablative material broke off before perforation measurements were made
 ** Piece of ablative material just about broken out. Large dia. measurement taken to edge of hole as if the piece has broken out.

TABLE II Cont't
IMPACT CHARACTERISTICS

Ablative Material Size	Back-up Thickness	Size	Material	PROJECTILE			ABLATIVE MATERIAL				BACK-UP		Remarks	Round #
				Impact Angle (Deg.)	Impact Vel. (ft/sec)	Normal Component of vel. (ft/sec)	Impact Energy Using Normal Vel. (kjoules)	Penetration (cm)	Hole Diameter (cm)	Minimum Dia (cm)	Area (cm ²)	Hole Diameter (cm)		
12"X13"X7/16" 124A	1" Al Honey-comb	Sphere 1/4" Dia	0.1560	90°	10,372 3,161	0.779	0.23*	0.75	0.75	0.58 (crater)	0.86	Not Perforated	Projectile fuzed in the ablative	5-3-60
12"X12"X7/16" 124A	"	"	0.1560	90°	11,755 3,583	1.001	0.32*	0.82	0.82	0.65 (crater)	0.91	"	Proj. was recovered	5-3-61
12"X12"X7/16" 124A	"	"	0.1560	90°	12,530 3,819	1.138	0.762*	0.92	0.88	0.71 (crater)	0.95	"	Proj fuzed in the ablative	5-3-62
12"X12"X7/16" 124A	"	"	0.1560	90°	13,405 4,086	1.302	2.0*	2.51	1.53	2.84 (crater)	1.90	"	Slight bulge on last Al plate	5-3-63
12"X12"X7/16" 124A	"	"	0.1560	90°	15,220 4,639	1.679	Perforation of Abl. only	2.86	2.48	2.39	5.81	2.72	Bulged last Al plate	5-3-64
12"X12"X7/16" 124A	"	"	0.1560	90°	16,360 4,987	1.940	Abl. Partially plated	2.67	2.	1.99	3.87	2.22	"	5-3-65
12"X12"X7/16" 124A	"	"	0.1560	90°	21,942 6,688	3.489	Perforation of Abl. only	6.0	3.2	13.42	4.13	"	"	5-3-66
12"X12"X7/16" 124A	"	"	0.1560	90°	21,599 6,583	3.380	"	4.21	3.73	13.87	4.20	"	**	5-3-67

* Penetration depth measured to the top of the projectile, normal to ablative surface.

** Bulged and loosened last Al plate from the honeycomb for about 1/2 the contact area.

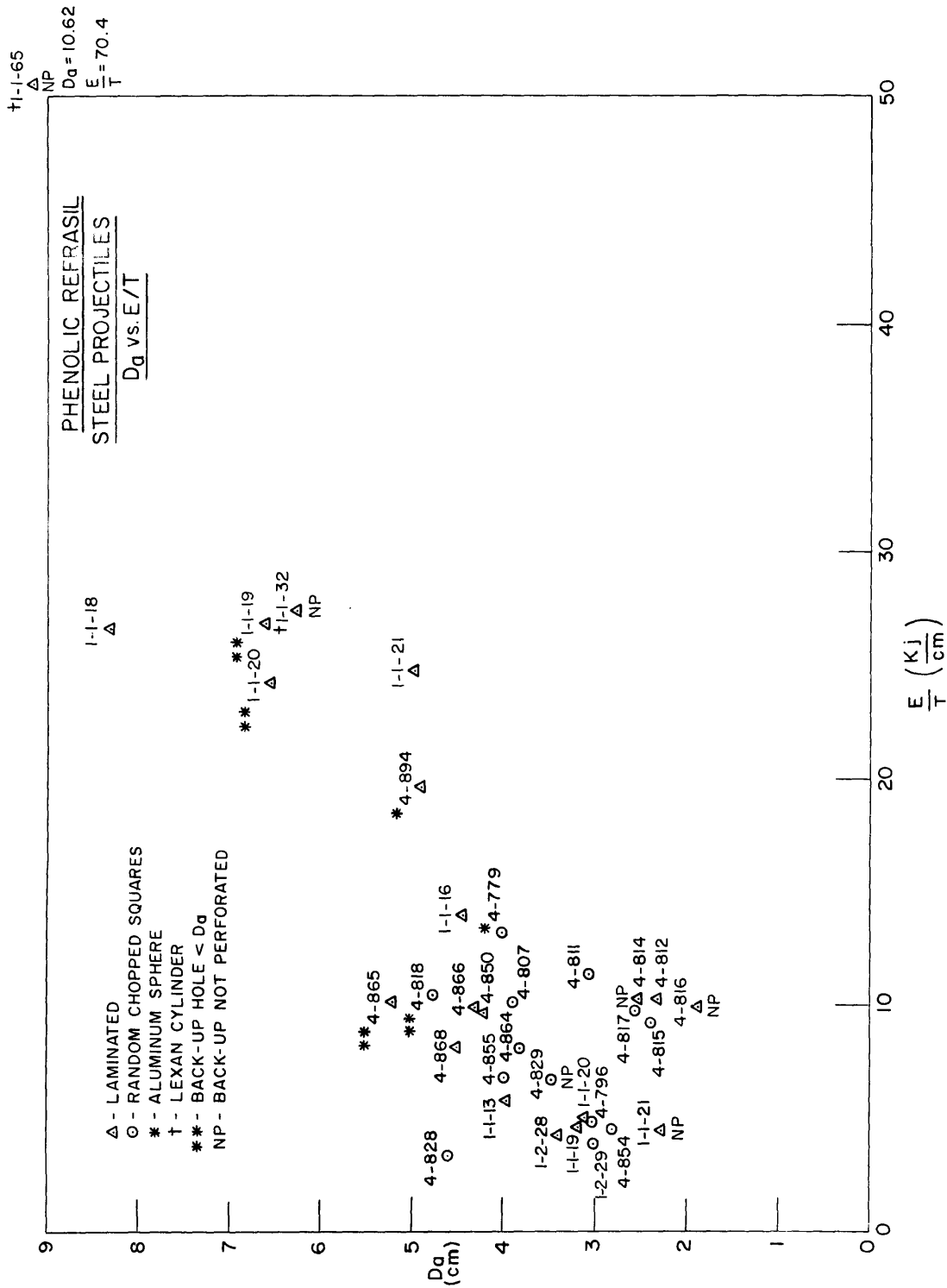


Fig. 1 - Hole size vs impact energy per unit of ablative thickness for phenolic refrasil

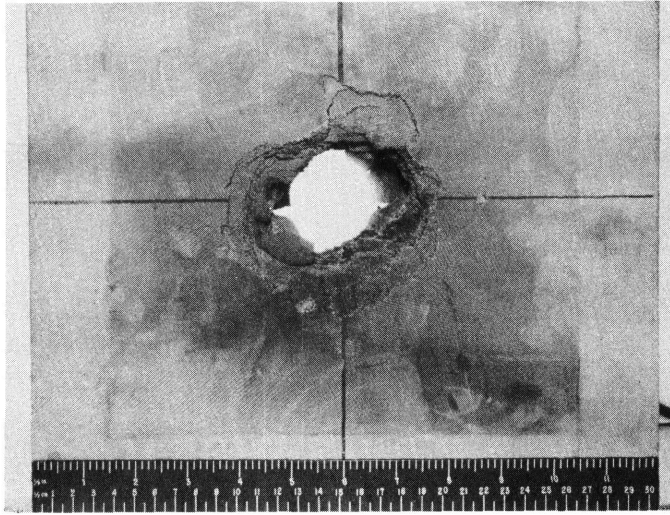


Figure 2(a) - Round No. 4-865 12"×12"×1" Laminated Astrolite with a 0.25" Al. back-up impacted at 90° with a 5-16" steel sphere (2.04 gm) at a velocity of 5.037 km/sec.

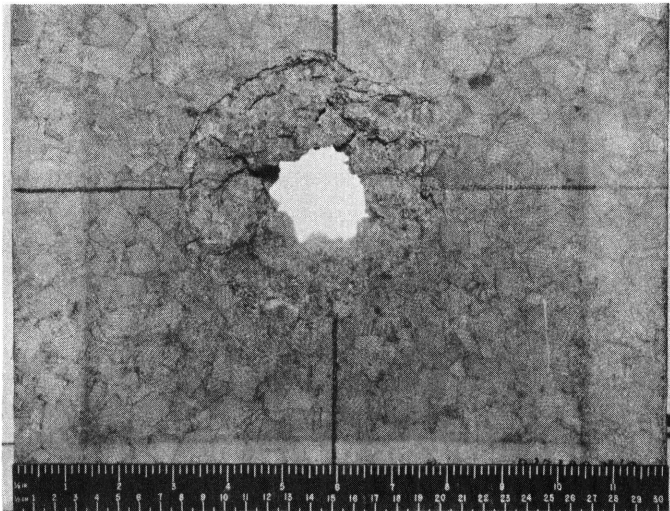
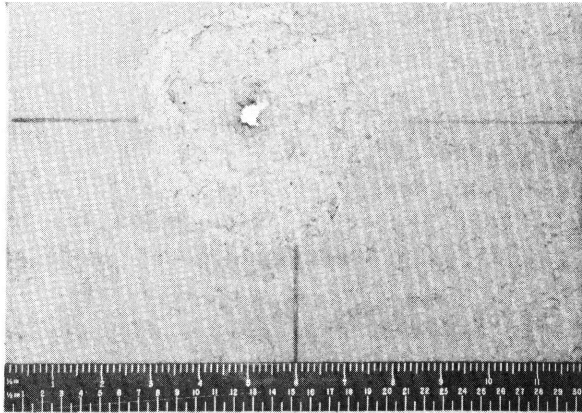
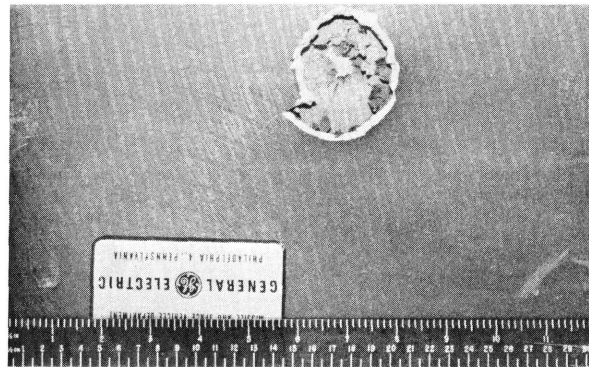


Figure 2(b) - Round No. 4-866 12"×12"×1" Random Chopped Squares Astrolite with a 0.25" Al. back-up impacted at 90° with a 5-16" steel sphere (2.04 gm) at a velocity of 4.970 km/sec.

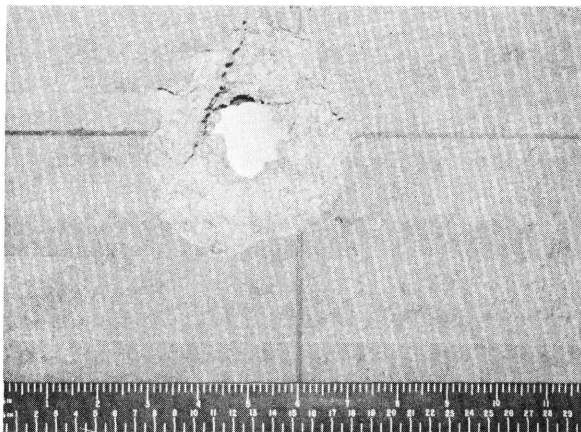


3(a) Top Front 4-851

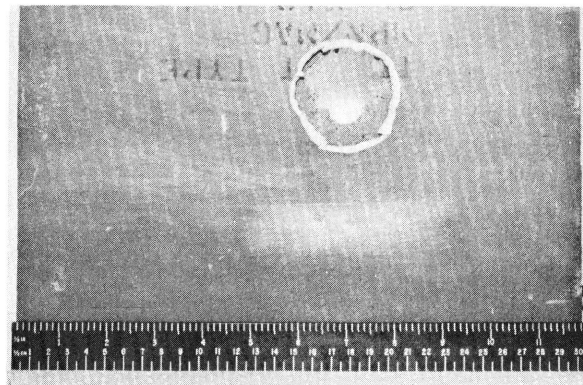


3(a) Top Rear 4-851

Figure 3(a) - Round No. 4-851 12"× 12"× 1" Random Chopped Squares Phenolic Nylon with a 0.25 Mg. back-up impacted at 90° with a 1/4" steel sphere (1.045 gm) at a velocity of 4.75 km/sec.



3(b) Top Front 4-852



3(b) Top Rear 4-852

Figure 3(b) - Round No. 4-852 12"× 12"× 1" Random Chopped Squares Phenolic Nylon with a 0.25" Mg. back-up impacted at 90° with a 1/4" steel sphere (1.045 gm) at a velocity of 4.75 km/sec.

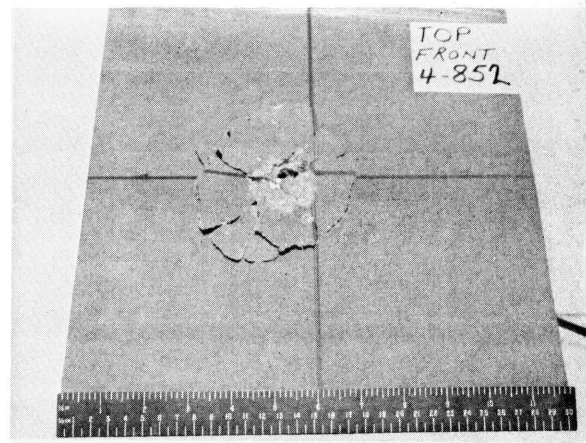
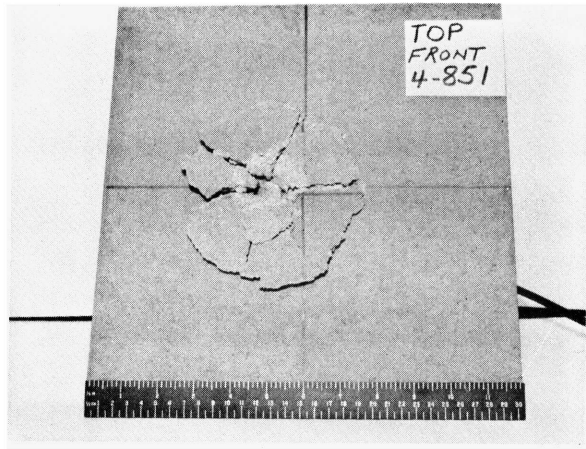


Figure 3(c) - Round No. 4-851 and 4-852. Recovered front spall pieces placed back into spall cavity after impact.

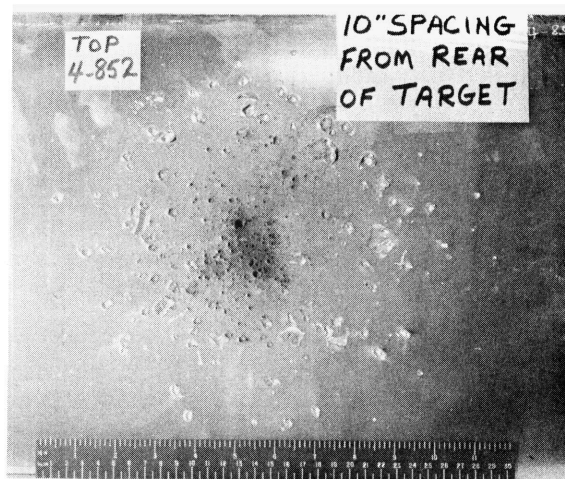
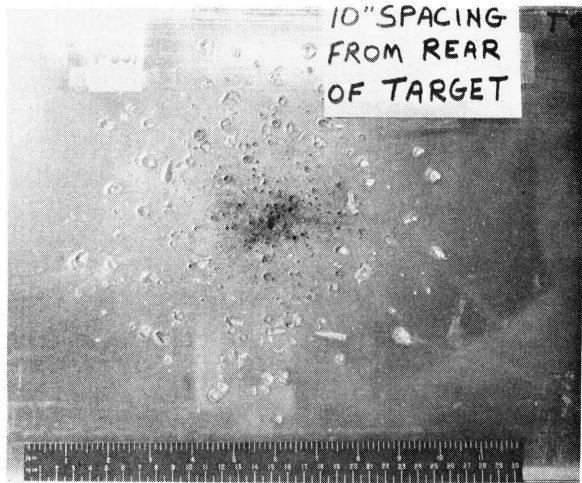


Figure 3(d) - Round No. 4-851 and 4-852. 0.25" thick 25 Aluminum witness plates placed 10" behind target.

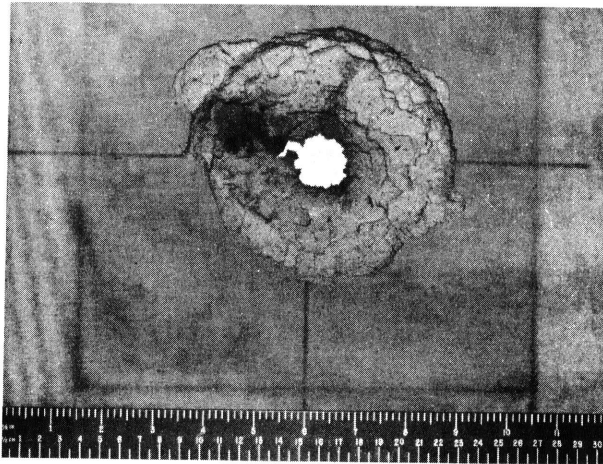


Figure 4(a) - Round No. 4-871.
12"×12"×1" Laminated Phenolic
Nylon with a 0.25" Al. back-up
impacted at 90° with a 5/16"
steel sphere (2.04 gm) at a ve-
locity of 5.0 km/sec.

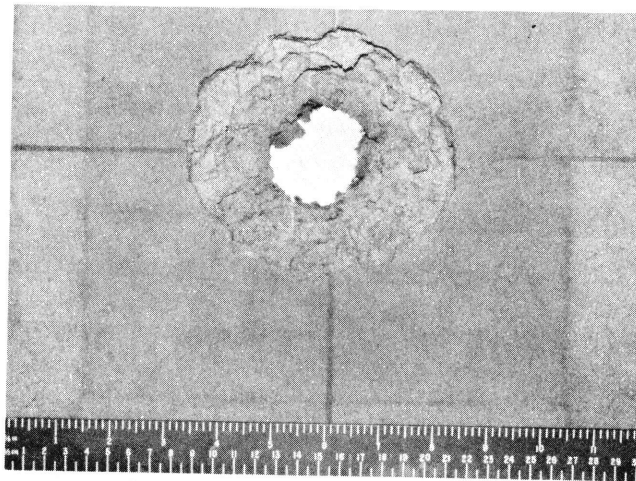


Figure 4(b) - Round No. 4-867.
12"×12"×1" Random Chopped
Squares Phenolic Nylon with a
0.25" Mg. back-up impacted at
90° with a 5/16" steel sphere
(2.04 gm) at a velocity of 4.54
km/sec.

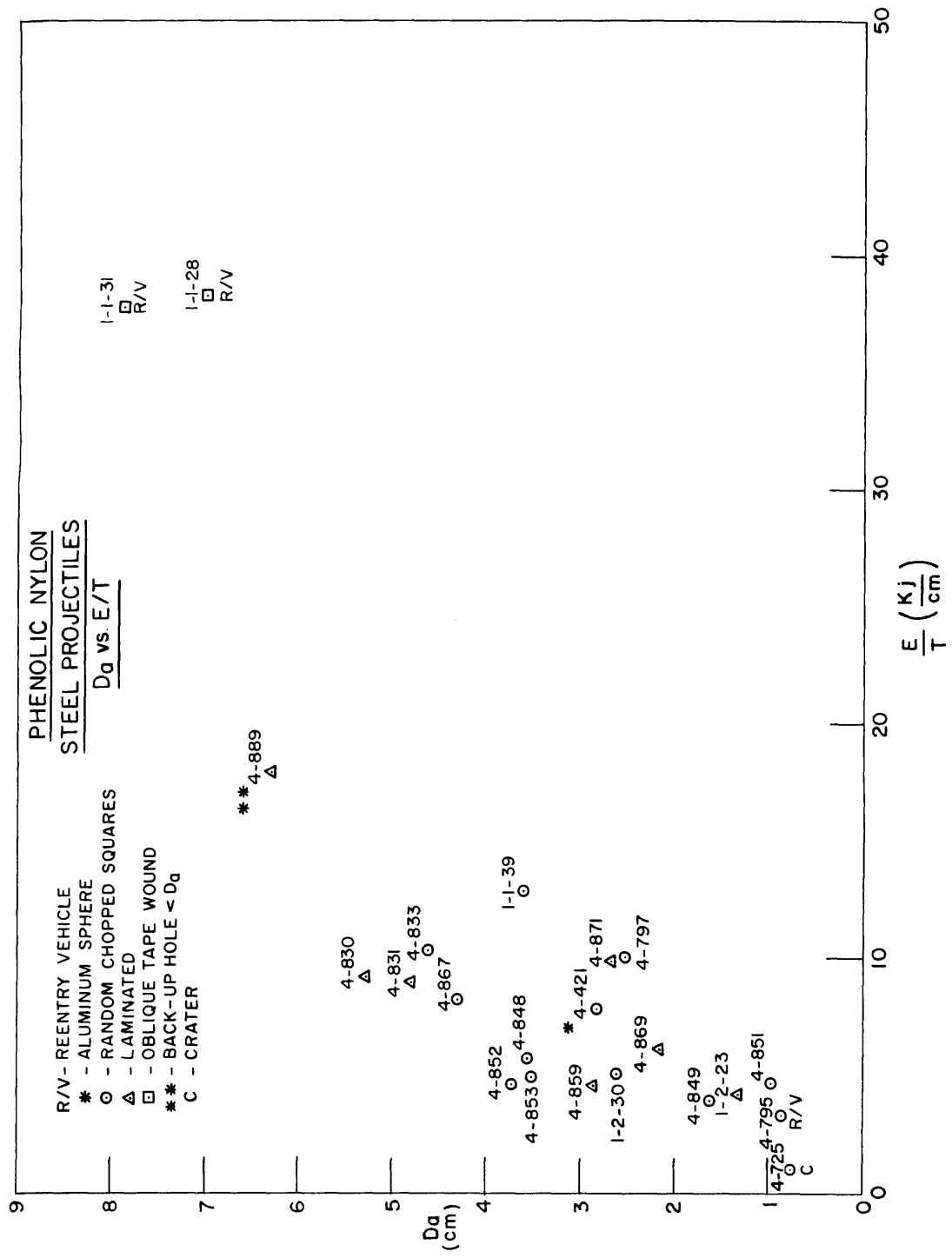


Fig. 5 - Hole size vs impact energy per unit of ablative thickness for phenolic nylon

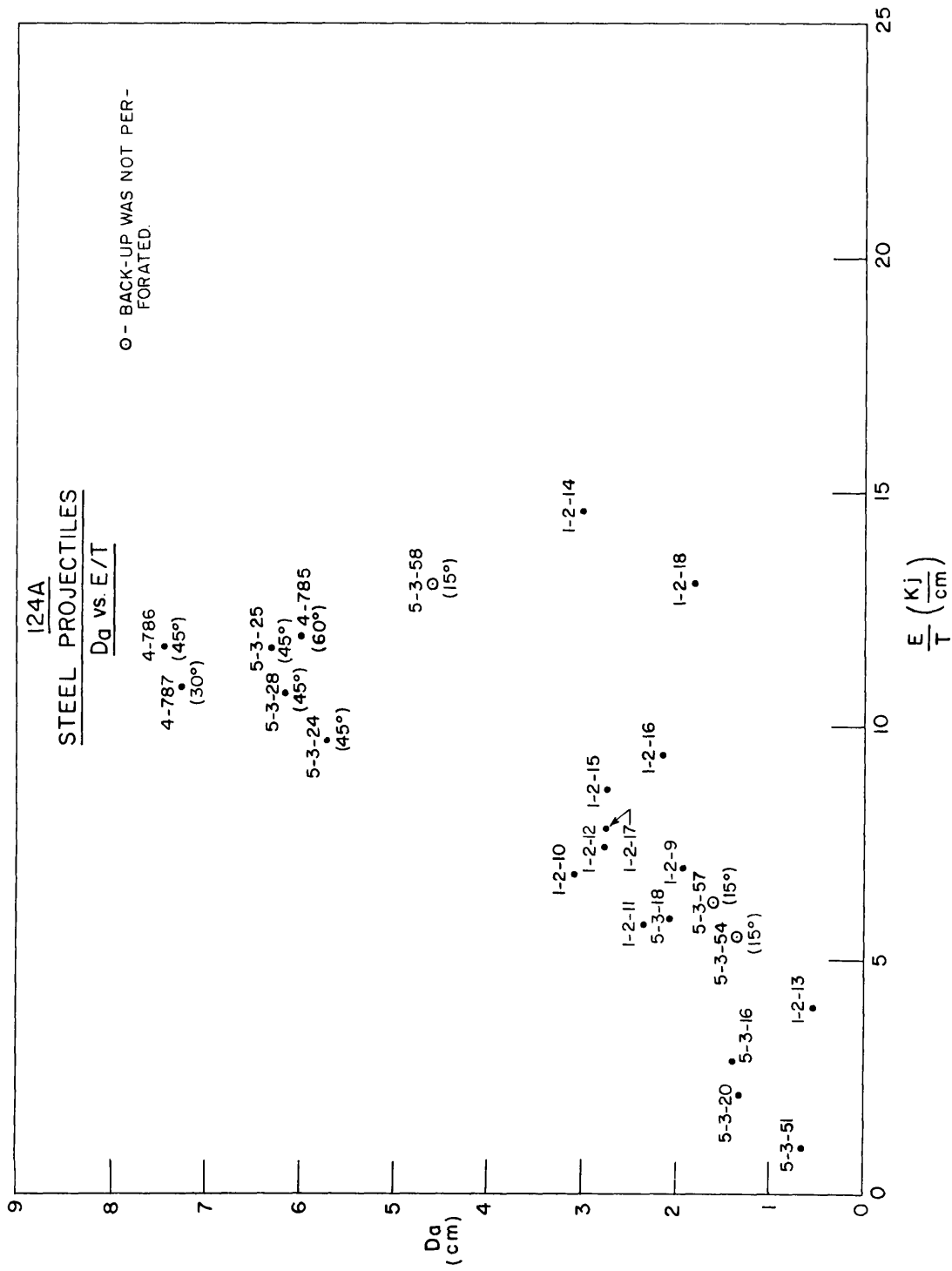


Fig. 6 - Hole size vs impact energy per unit of ablative thickness for G.E. 124A

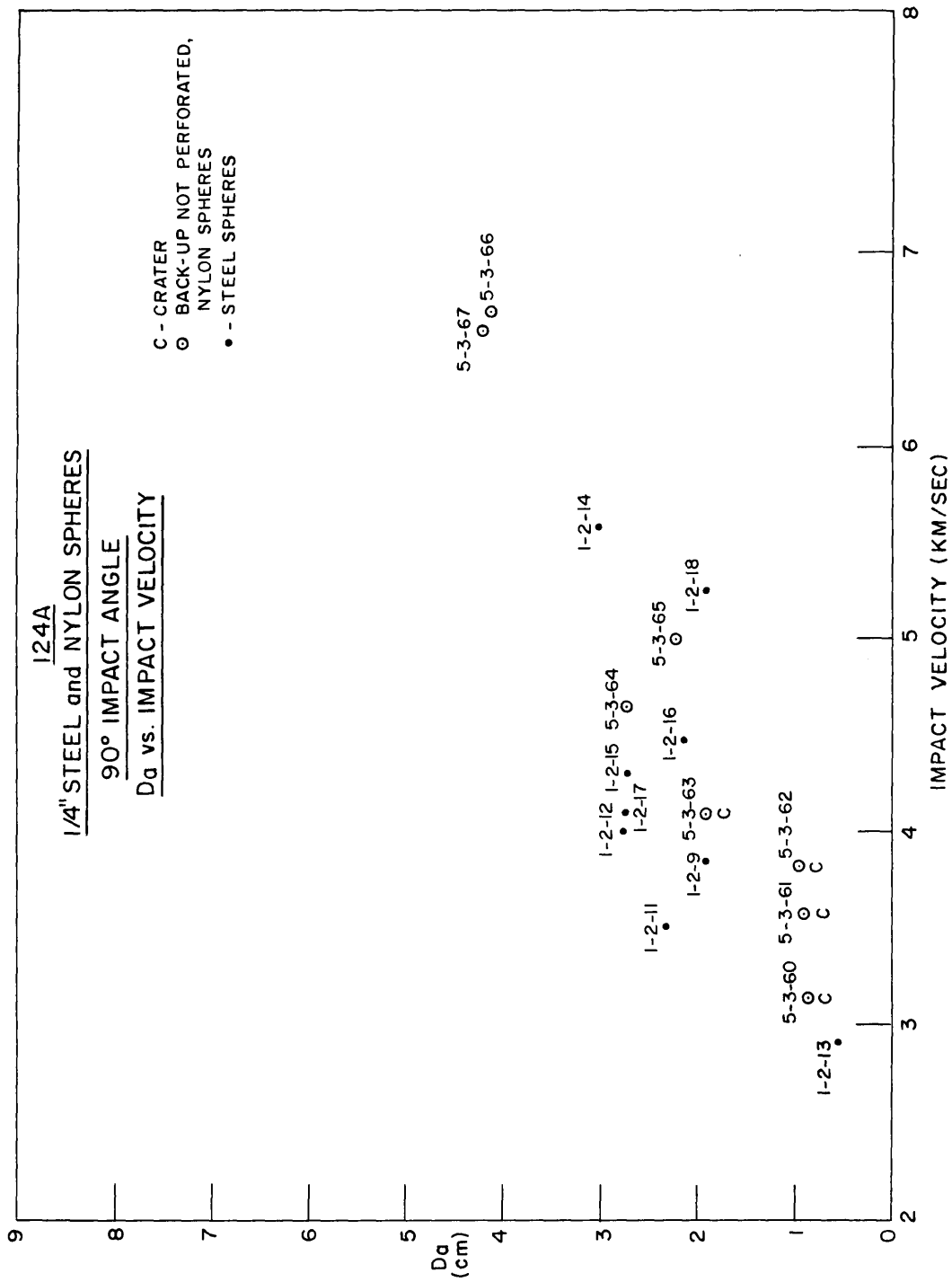


Fig. 7 - Hole size vs impact velocity (1/4-in. steel and nylon spheres) for G.E. 124A

SECTION II
Impact Damage By Large Mass Materials

C.D. Porter
J. Davis

August 1963

Dynamics Branch, Mechanics Division
U.S. NAVAL RESEARCH LABORATORY
WASHINGTON, D.C.

B'

PROBLEM STATUS

This is a Quarterly Technical Progress Report.
Work on this Project is continuing.

AUTHORIZATION

NRL Problem 62F04-11C

ARPA Order No.149-60

LIST OF FIGURES

FIGURE

1. Target Layout of Shot 1 (8.2", 2.5-inch gun)
2. Vertical Section Through Mark IV Target at Impact Point
3. View of Target at Impact
4. View of Target 320 Microseconds After Impact
- 5a. Structural Deformation of Target in Impact Zone
- 5b. Structural Deformation of Target in Impact Zone (Schematic)
6. 40-MM High Pressure Case and Core Section (Prototype Shot for 2nd 8.2" Shot)
7. Details of Ring Seal Sabot (40-MM, .50-Cal.)
8. Velocity Station Shadowgraph of .5" Sphere
9. Weighted Hydraulic Piston
10. Photographic View of Petal and Slider Valves for 8.2" Gun (from compression tube side)
11. Petal Valve Diaphragm
12. Petal Valve Diaphragm with 22° Control Lines (Schematic)
13. Petal Valve Diaphragm with 22° Control Lines (Fig. 13)

SUMMARY

Preliminary work in structural analysis of the MK IV nose cone impacted with 253-gm Lexan cylinder at 5.6 KM/Sec indicates that about 1% or more of the projectile energy was transmitted to the remaining portion of the structure. This 1% appears sufficient to account for the severe delamination of about 50% of the ablative material. Transverse wave propagation as indicated by breakaway of a light shield appears to be the mechanism for the major portion of energy transferred to the structure.

Improvements in large gun accelerator techniques are: the development of a ring-seal type sabot, the improvement of the NOL petal valve, and the development of a low-friction, hydraulic piston.

Future impact studies and instrumentation are discussed.

INTRODUCTION

The impact program using the new 8.2-inch hypervelocity gun (1, 2) was started in early March. The objective of this program is to study the effect of large, dense, concentrated and distributed masses on impact damage.

Observations on the structural aspects of impact damage is reported. Much of the analysis of the damage on the first target has been done during this period for purposes of determining the type of instrumentation needed in the structural and distributed mass studies.

Areas where improvements have been made in the accelerator are also discussed.

IMPACT ANALYSIS

Optical

A Fastex framing camera was mounted to view, during impact, an elliptical sector of the Mark IV nose cone with the major axis of about 30 inches and minor axis of about 20 inches. Figure 1 is a schematic plan view of the Mark IV target in the target chamber. The front of the target was suspended by means of cushioned studs welded into the chamber wall. The rear was hung by a cable suspension to overhead rings. Impact was planned on the cylindrical section 6-inches ahead of the main steel reinforcing ring, which connects the cylindrical section to the first conical section. The forward tip of the viewed section is approximately the same distance from the reinforcing ring and 90° from the impact point. A 1-inch thick celotex light-shield was placed completely around the impact area. The exposed areas were sealed with tape to avoid overexposing the film during the early phases of impact.

Figure 2 is a sectional view of the target at the point of impact. The sector viewed by the overhead camera and the section of the impact flash shield are also shown. Of particular interest is the arc length (14.3 inches) from the impact point to the taped joint topside of the upper flash shield.

Color film was used to gain an idea of the color of the major visual radiation from the impact as well as to gain some idea of the velocity of the gas particles. The faster the gas jets and dust particles travel, the nearer the radiation from the residue air wake approaches the ultraviolet region.

The first view, Figure 3, is taken at the start of target impact by impact flash seeping around the loose taped joints. In the colored photo of this phenomenon the almost blue light, available in high intensity only for a few micro-seconds after impact, was noted. The squares on the viewed section are of two-inch size, and the marked area (viewed section) is only a small sector of the target which is too large for full coverage.

In the next frame (not shown), 160 micro-seconds later, the light had already decayed below visibility, except for a small area at the forward part of the viewed section which flowed yellow from gases which were flowing through a break-away from the taped shield and target.

In the next frame (Figure 4) 320 micro-seconds later, the lower edge of the light shield and contacting target had completed its break-up exposing large areas to the direct-viewing of the heated gas composed of the lower intensity target dust and residue target chamber atmosphere.

In the upper left portion one notes luminous linear streaks, some of which are a foot long, which do not show the turbulence of gas flow. It is believed these are the radiant wakes left by particles sprayed back from the impact crater and traveling at high speed through the rarefied air.

Considering the onset of edge-seal break-up as occurring in the 130-160 micro-second period between frames, one can calculate the velocity of the disturbance propagated over the 14.3-inch path as lying between 2.27 km/sec and 2.80 km/sec. The measured longitudinal wave velocity lies between 3.23 km/sec and 4.41 km/sec depending upon direction of propagation in the material fibers. The transverse wave propagation velocity has not been verified for the composite sandwich. The velocity range calculated from photographic observation could be that of the transverse wave because the velocity of transverse propagation is considerably lower than that of the longitudinal mode.

STRUCTURAL ANALYSIS

Evidence of structural absorption of the projectile energy is contained in the ruptured and bent structural ring member and deformed lips around the hole as shown in Figure 5. Analysis of this work of bending shear and non-elastic stretching shows that at least 40 kilojoules of energy was absorbed in performance of this work. A reasonable assumption is that this deformation energy may be linearly related to the energy actually transmitted to the target shell structure around the hole which

was responsible for the severe delamination observed. The projectile possessed about 3,940 kilojoules of kinetic energy. The known deformation energy is a little over 1% of the impact energy. If an equivalent amount of kinetic energy reached the structure, this energy in potential form is equivalent to loading the structure with 14,000 kilograms over the hole area with a resultant deformation of 28 cm. Such deformation would definitely crack and delaminate the ablative (Tape Wound Refrasil). Large pieces of ablative material weighing 9.38 kg cracked off beyond the hole area and were recovered. This is a complete breakoff of about 11.5% of the ablative surface beyond the hole area, which is 3.0% of the surface. Loose strips comprising about 35% of the surface would have broken off quickly in the slipstream around a re-entry vehicle during flight.

This added damage could be the result of structural deformation and vibrations and is an aspect of damage that has not been observed in previously controlled flat-plate experiments. This aspect of damage may have considerable bearing upon the ability of an impacting mass to kill an incoming missile. The preliminary study adds considerable impetus to the effort to improve the instrumentation upon the target. A break-screen network may be devised to analyze the wave velocity behavior in an impacted structural target.

ACCELERATOR TECHNIQUE DEVELOPMENT

Large Gun Prototype

Every 8.2-inch gun firing, involving changes which may increase gun stresses, is duplicated parameterwise on a 40-mm gun whose high-pressure section and core duplicate in 1/5 scale every detail of the respective sections of the 8.2-inch gun. The high-pressure case and high-pressure core are shown in Figure 6.

Parameters similar to the next 8.2-inch gun shot selected for the prototype firing are as follows:

	<u>40-MM Prototype</u>	<u>8.2"LG-Gun</u>
Piston Size	1.63"OD x 12"	8.2"OD x 60"
Piston Weight	411.6 gm	113.5 lb
Projectile Size	.5" Al Sphere	2.45" Al Sphere
Projectile Weight	3.01 gm	361 gm
Ring-Seal Type		
Sabot	.122 gm	15.2 gm
Powder	150-gm, 20mm + 135-gm, 40mm	851b, 6"*
Propellant Pressure	42,000 psi	40,000 psi
Driver Gas	210 psi H ₂	210 psi H ₂
Projectile Velocity	19,000 fps	21,000 fps

* Propellant weight increased to give a greater projectile velocity.

Ring Seal Sabot Development

40-MM, 50-Cal. Prototype.

A feature of this shot was the ring-seal type of sabot designed to give a lightweight self-stripping support to the 1/2-inch aluminum sphere. If launch tube cross sectional area is A, sphere cross-sectional area is S, sphere mass is M_p and sabot mass is M_s then allowing for a narrow band of friction in the area near maximum ball diameter, it can be shown that if

$$\frac{M_s}{M_p} < \frac{A - S}{1.1 (S)}$$

then sabot and ball should accelerate together.

To make the sabot light as possible (about 4% of sphere mass) there must be little clearance between ball and the launch tube bore. A ring-seal sabot was developed on this basis for the 40-mm prototype as shown in Figure 7. Figure 8 shows the half-inch, 3.01-gm ball stripped of the sabot material as it passed the velocity stations, 2' apart, at 18,961 fps.

Hydraulic Piston

One feature of the prototype shot was the addition of packed steel wool about the stem of the hydraulic piston, Figure 9, to add the piston weight needed with the heavier projectile and to keep friction and distortion down. The packed steel-wool is carefully taped so that the wool is separated from the wall by a layer of water. About 30% of the piston weight is plastic, 22% steel-wool and the remaining 48% water.

Petal Valve

After analyzing the results of the first shot of the 8.2, 2.5-inch hypervelocity gun, it was decided that the slider-type break valve should be replaced with a petaling diaphragm valve. (Figure 10)

The advantages which the petal valve has over the slider-valve are: the break pressure of the petal valve is unaffected by pressures applied by surrounding core parts; the opening and opened phases of the petal valve nozzle are aerodynamically more desirable; there is less tendency to close; and there is a reduction in machining time and cost. The disadvantage of using a large petal valve has been the breaking off of pieces of valve material which would damage the projectile and launch tube.

A dynamic valve tester was designed which would duplicate the valve section of the 8.2, 2.5-inch gun. The first test-valve was made using the NO_L design parameters.⁽³⁾ Examination after testing showed a ragged break which seemed to be inclined at a 45-degree angle. (Figure 11) The total mass-loss by weight was 2.95 grams. The second test-valve was altered from the first by adding a small control line at the bottom of the major slots with the hope of reducing the raggedness of the break and the mass-loss. Examination after the shot again showed a ragged break which was inclined at a 45 degree angle. The mass loss was 1.77 grams.

After two valves, whose breaks were inclined on a 45-degree angle, it was concluded that the material was failing in shear with the maximum shearing stress occurring on the cross-section inclined at 45 degrees. This phenomenon occurs in certain types of materials.

From the above observations it was concluded that the failure should be controlled to be a smooth break inclined at a 45 degree angle. This was attempted by putting control lines on the side opposite the major break slots off-set at a 45-degree angle. Valves from the third test were measured to determine the amount of plastic deformation before the start of the shear-type of failure. From the deformation measurements the control lines were relocated at an angle of about 22 degrees measured from the perpendicular cross-section-line through the major slot. (Figure 12)

This fourth test valve functioned as desired. The break followed the control lines giving a smooth break with no noticeable pieces missing (Figure 13). The mass-loss by weight was 0.17 grams or 0.01% of the total valve weight. The measured break pressure was 75,210 psi compared to the desired break pressure 75,000 psi. The functioning of test valve No. 4 was deemed satisfactory and a duplicate will be used in the 8.2, 2.5-inch gun for shot No. 2.

FUTURE WORK

Instrumentation

A 4' x 4' x 1 1/2" ablative target with 1/4" steel back-up is being set-up at 90° incidence to study mass scaling effects on thick ablative targets.

Specific instrumentation planned includes:

(1) Orthogonal flash X-ray units to view back of target after the steel back-up plate opens up.

(2) A shadowgraph system to obtain velocity of petaling plate after impact during the petaling action of the back-up.

(3) Chronograph screens to measure the velocity of the fastest particle as it proceeds through a system of screens set at various points in a maftex-plywood witness array in which particle recovery will also be carried out.

(4) Delicate screens will be placed about the impact point in the ablative materials to study the wave propagation velocity. An attempt will be made to differentiate between the longitudinal and shear modes of wave propagation.

(5) Accelerometers will be placed in the areas where they will not be damaged to get a better idea of energy absorbed by the structure.

(6) Two new vertical viewing systems will provide orthogonal views of the projectile array for future distributed mass studies.

Density Effect Study

An effort will be made to use the ring-type sabot to accelerate dense materials.

REFERENCES

1. Proceedings of the Sixth Hypervelocity Impact Symposium, May 1963, Cleveland, Ohio. "Hypervelocity Impact Into Ablative Materials" by M.A. Persechino.
2. Progress Report No. 11, Hypervelocity Kill Mechanisms Program, NRL Report No. 5990 - Semiannual Progress for Period Ending March 20, 1963, Section B.
3. Rast, J.J., NAVORD Report 6865, January 1961.

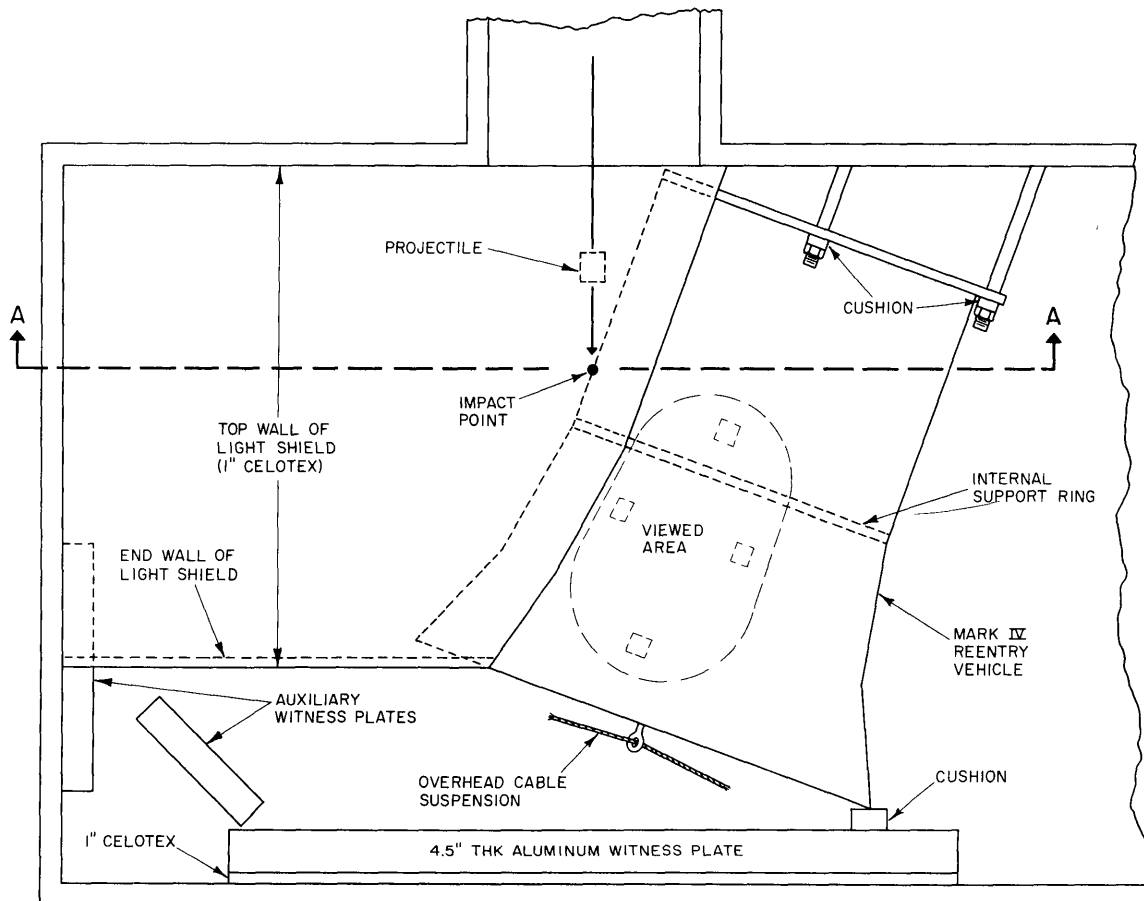


Figure 1 - Target layout of shot 1 (8.2-inch, 2.5-inch gun)

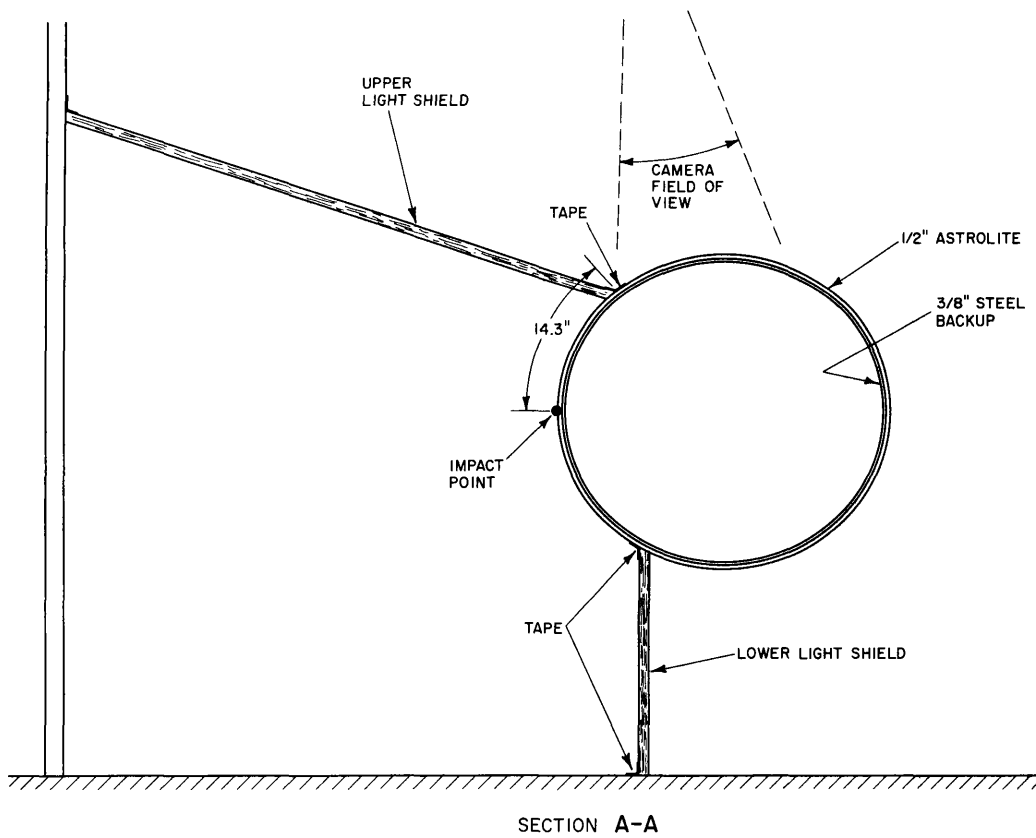


Figure 2 - Vertical section through Mark IV target at impact point

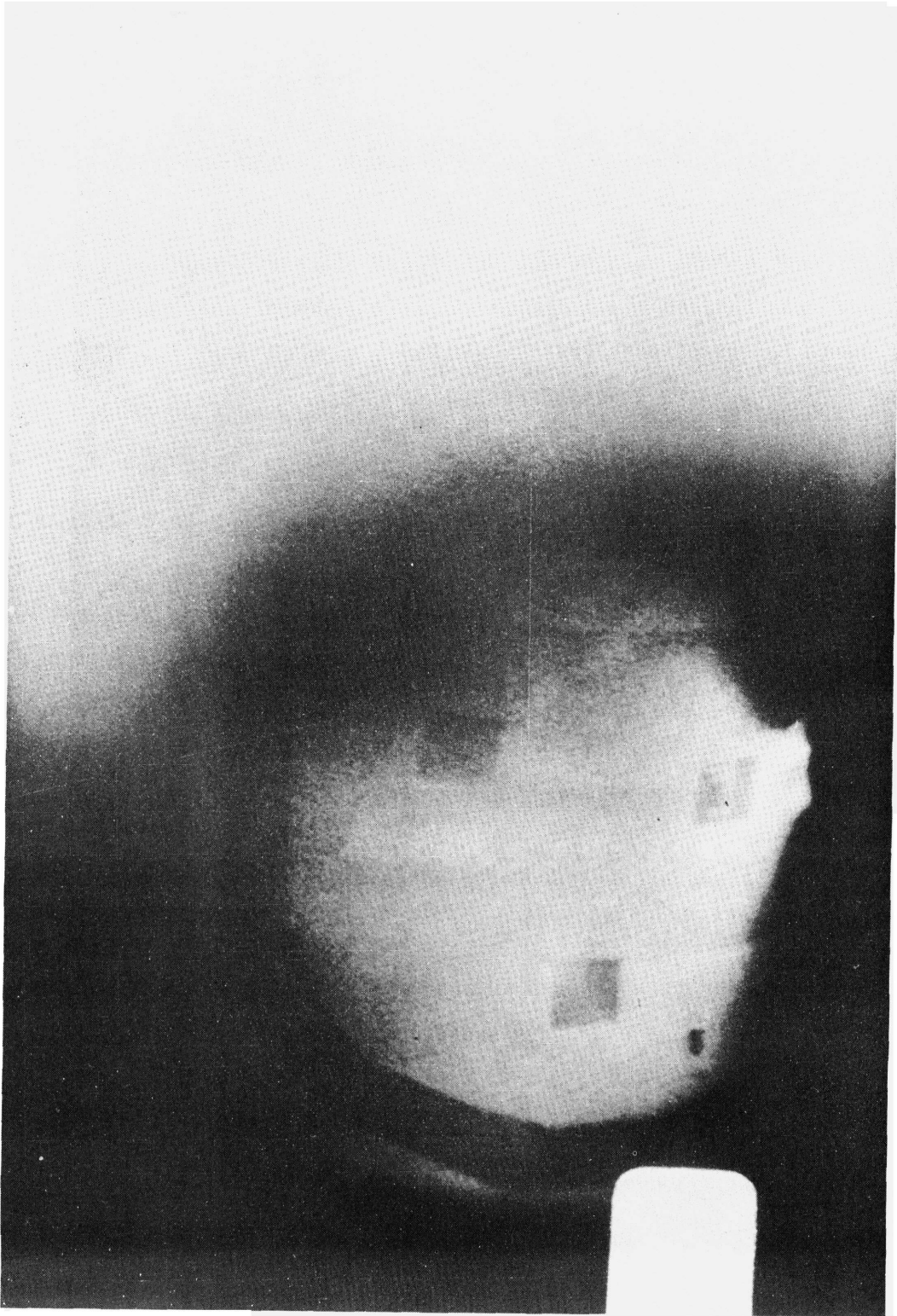


Figure 3 - View of target at impact

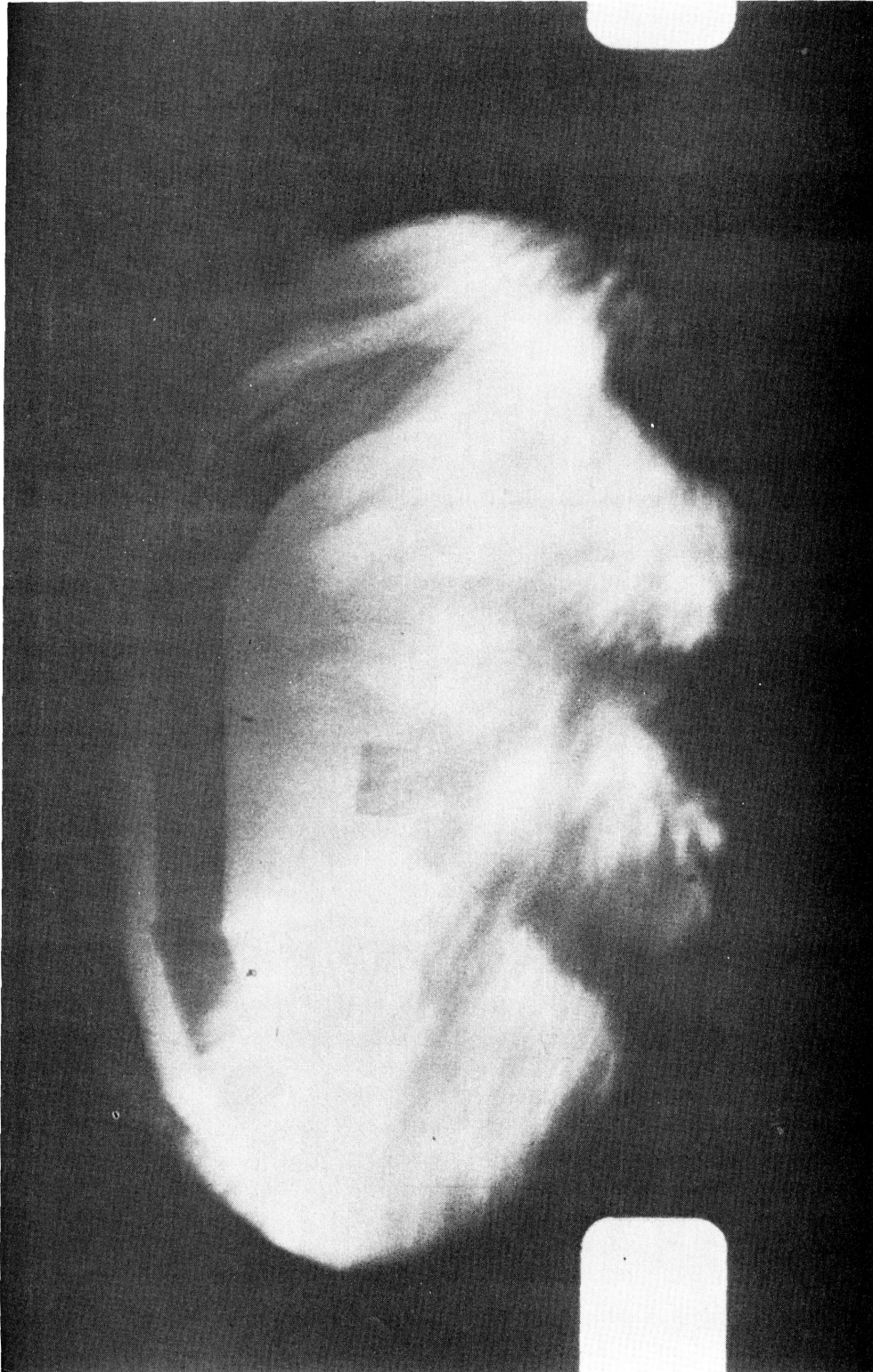


Figure 4 - View of target 320 microseconds after impact

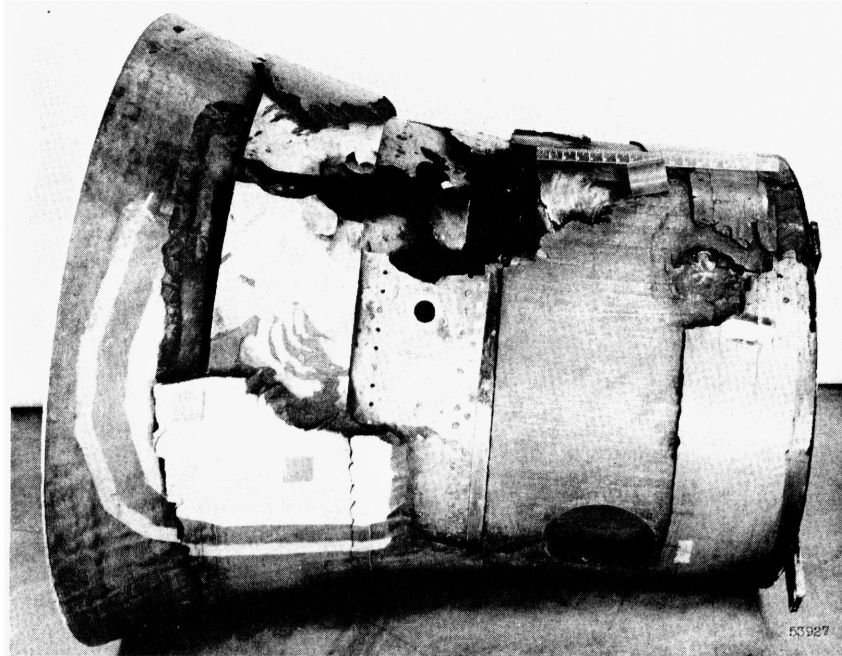


Figure 5a - Structural deformation of target in impact zone

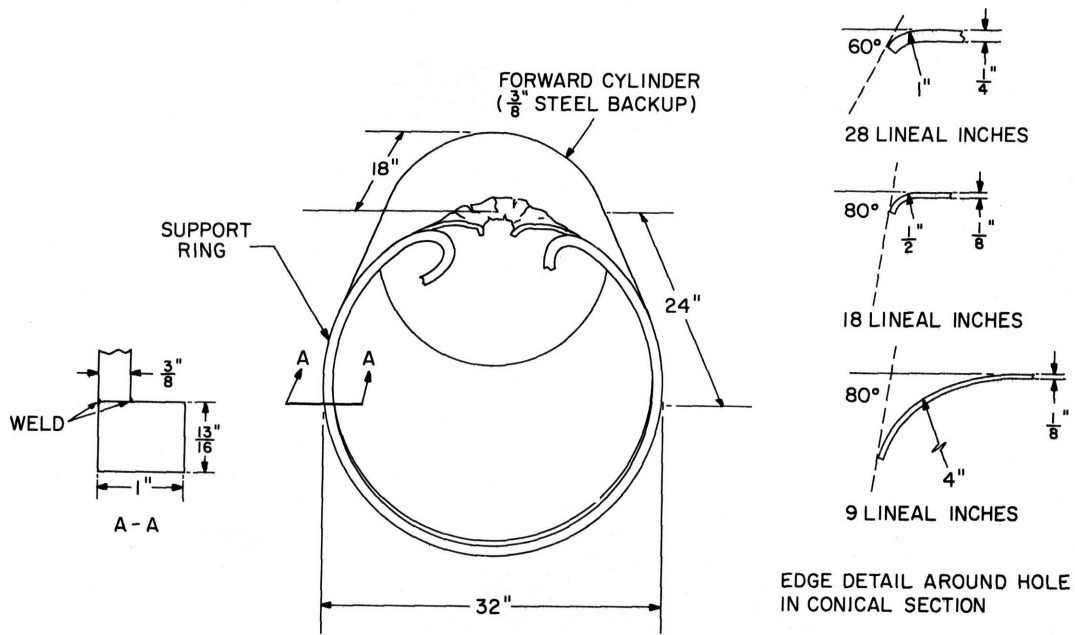


Figure 5b - Structural deformation of target in impact zone

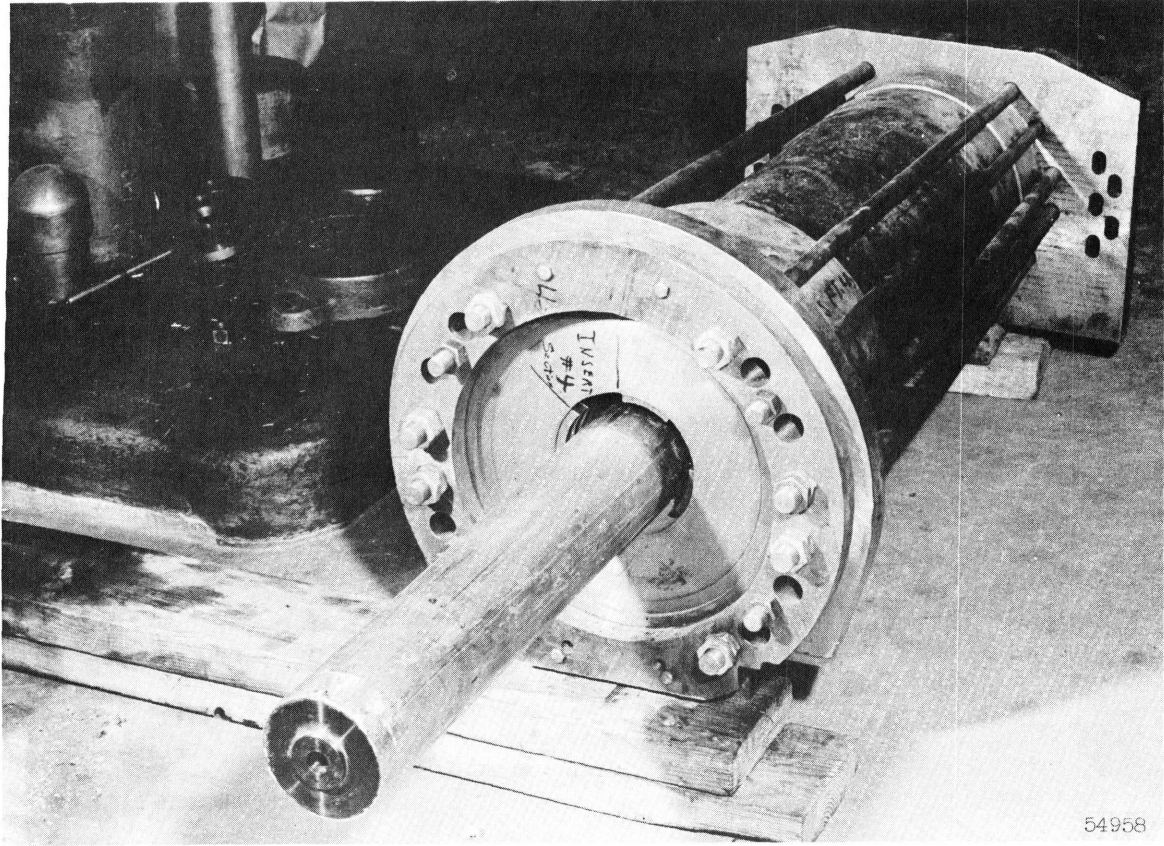


Figure 6 - 40 mm high pressure case and core section
(prototype shot for 2nd 8.2-inch shot)

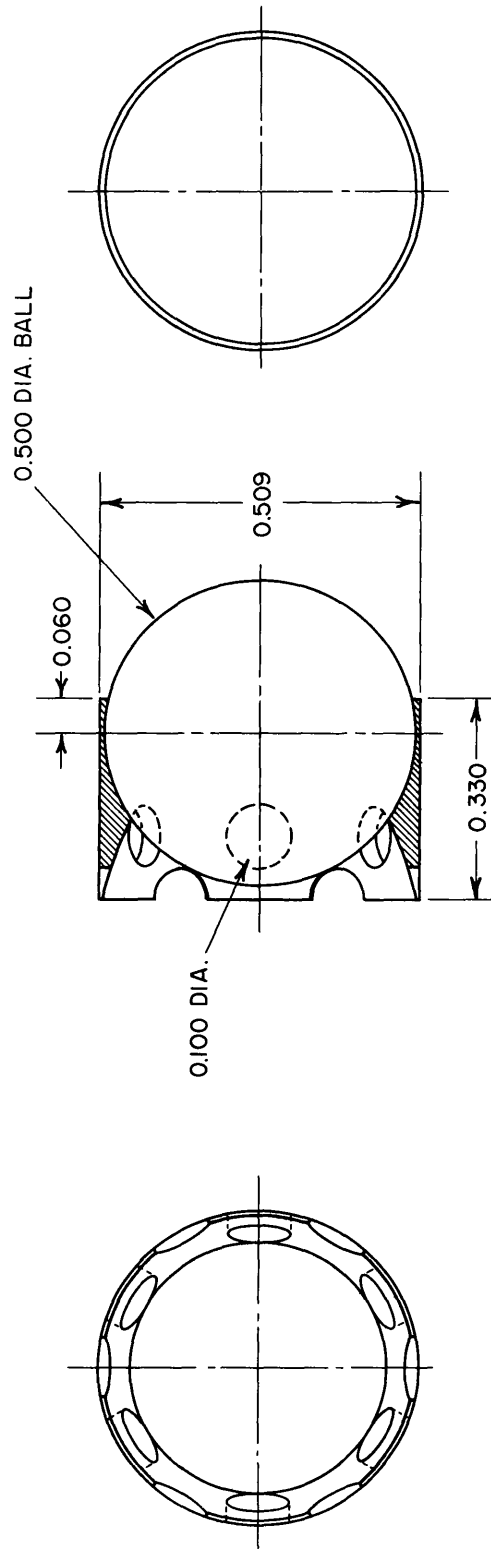


Figure 7 - Details of ring seal sabot (40 mm, .50 Cal.)

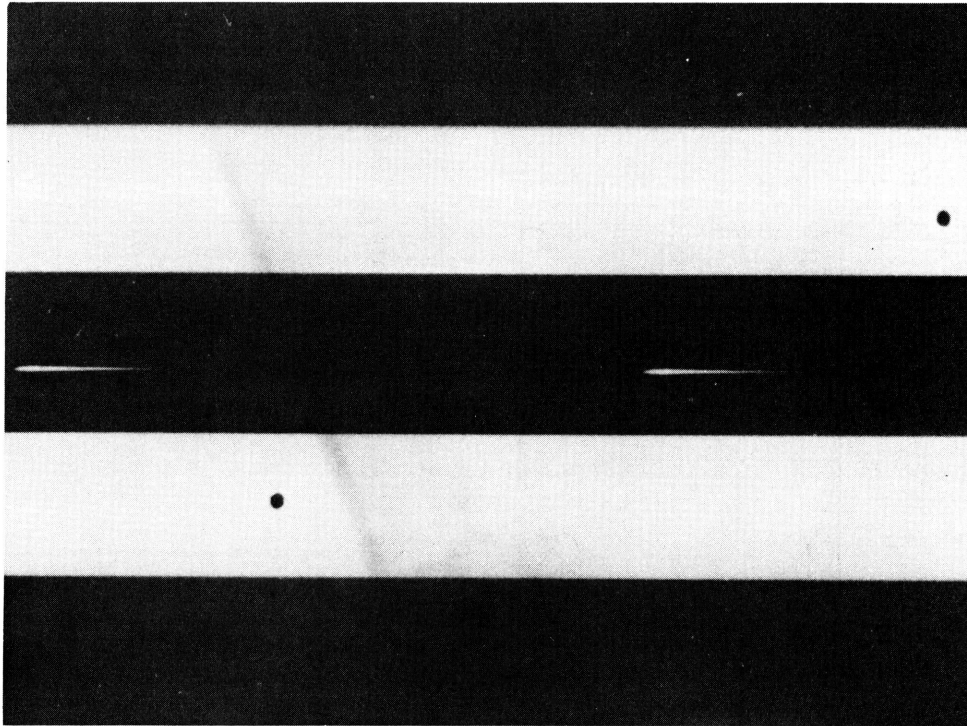


Figure 8 - Velocity station shadowgraph of .5-inch sphere

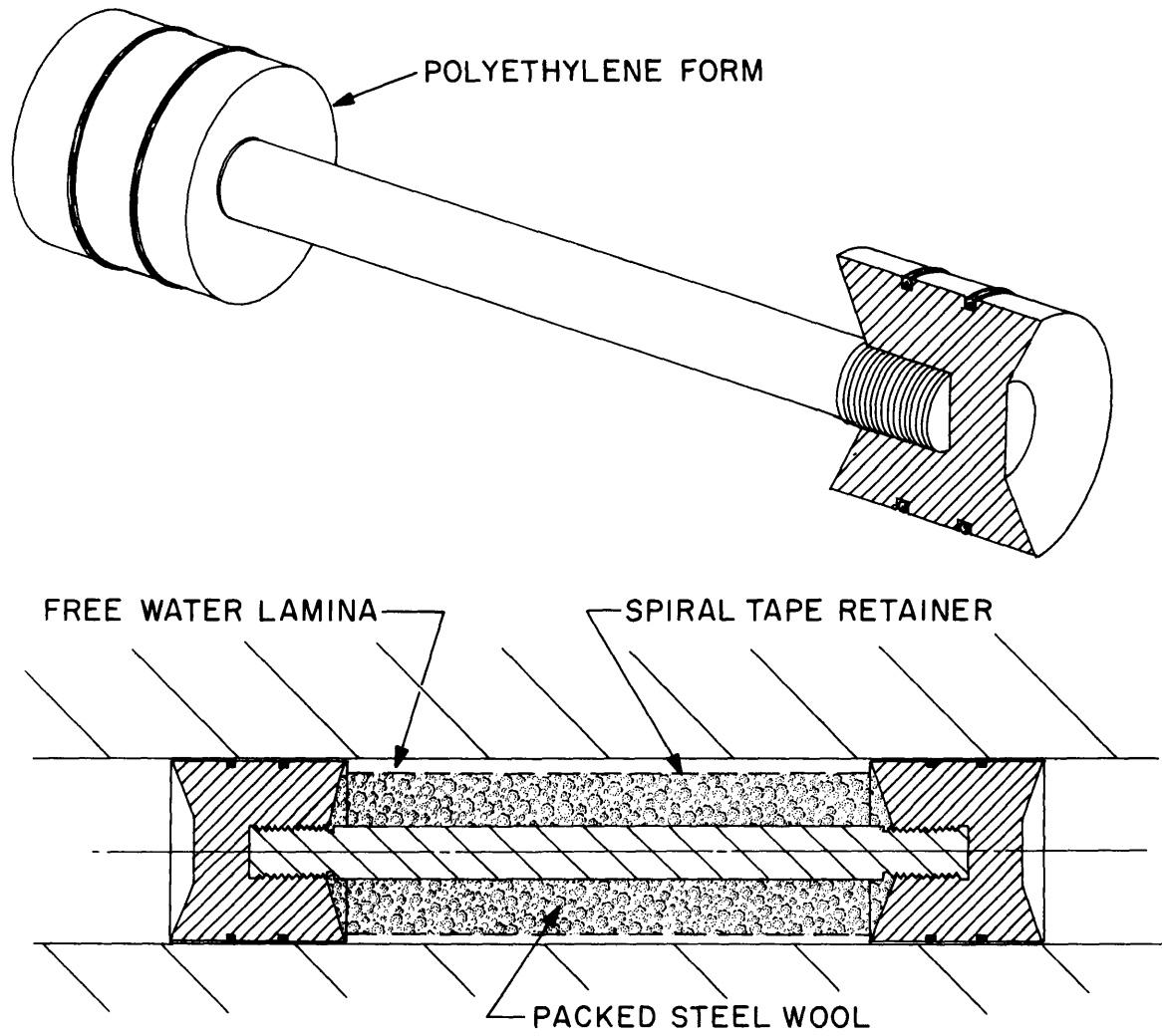
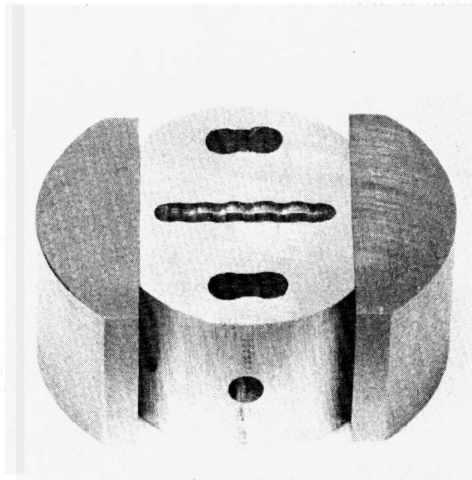
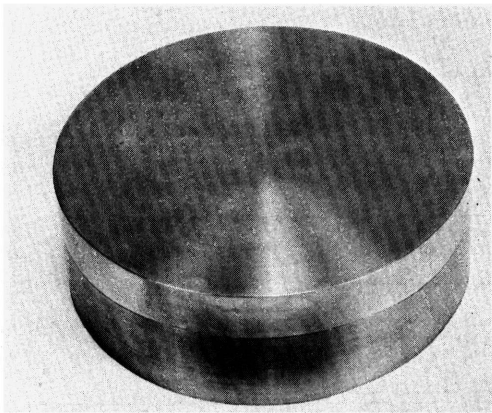
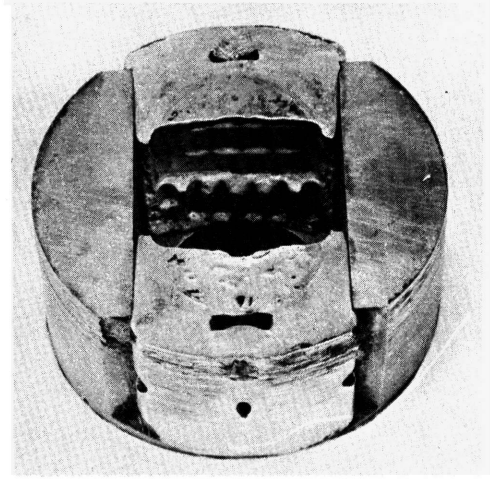


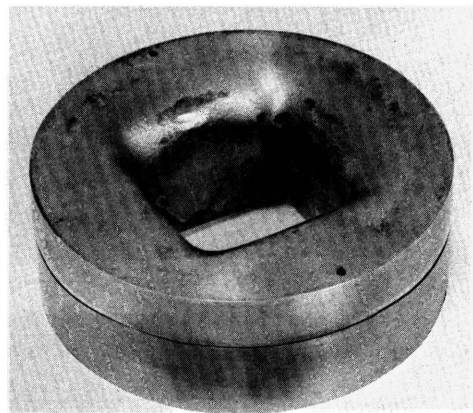
Figure 9 - Weighted hydraulic piston



← SLIDER VALVE →



← PETAL VALVE →



BEFORE FUNCTIONING

AFTER FUNCTIONING

Figure 10 - Photographic view of petal and slider valves for 8.2-inch, 25-inch HV gun (from compression tube side)



Figure 11 - Petal valve diaphragm with 22° control lines

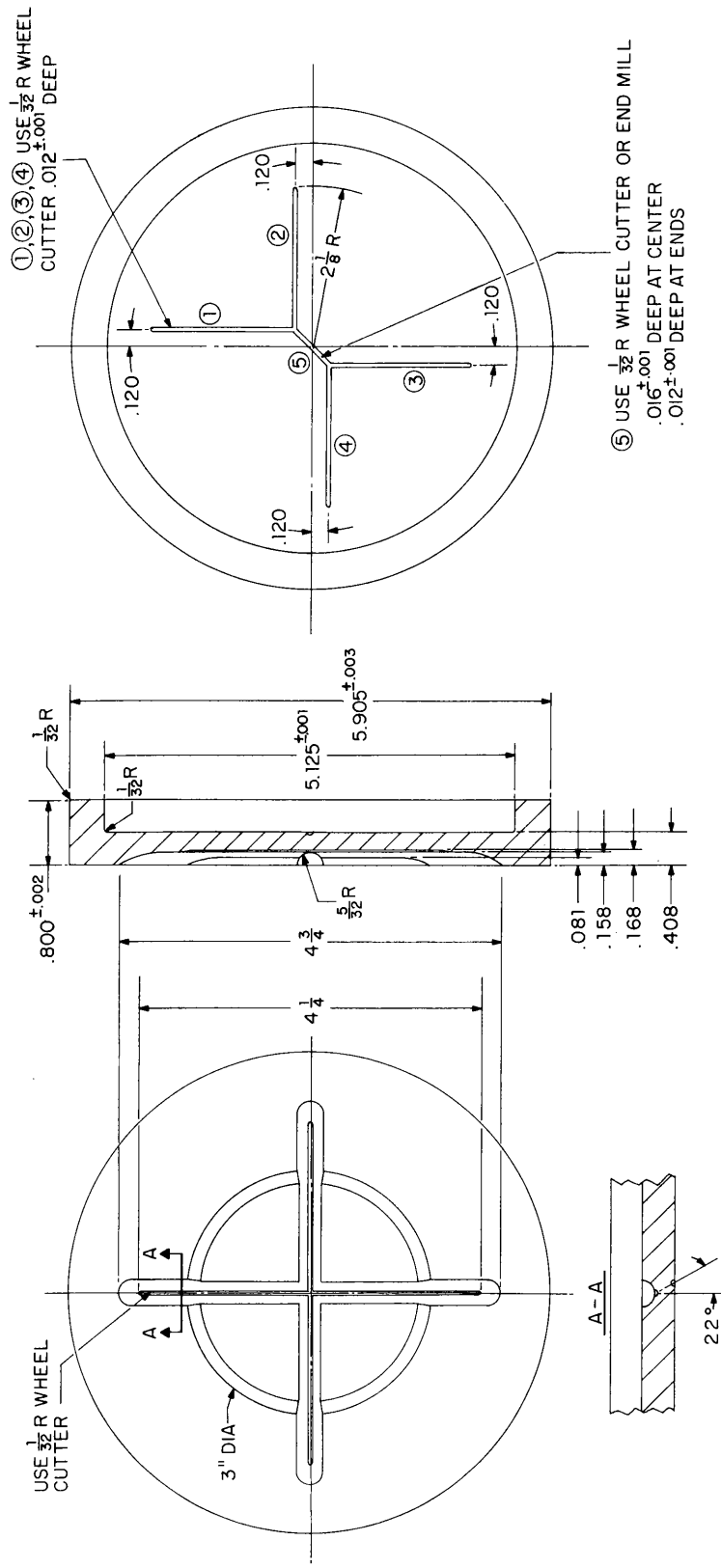


Figure 12 - Petaling diaphragm valve No. 4

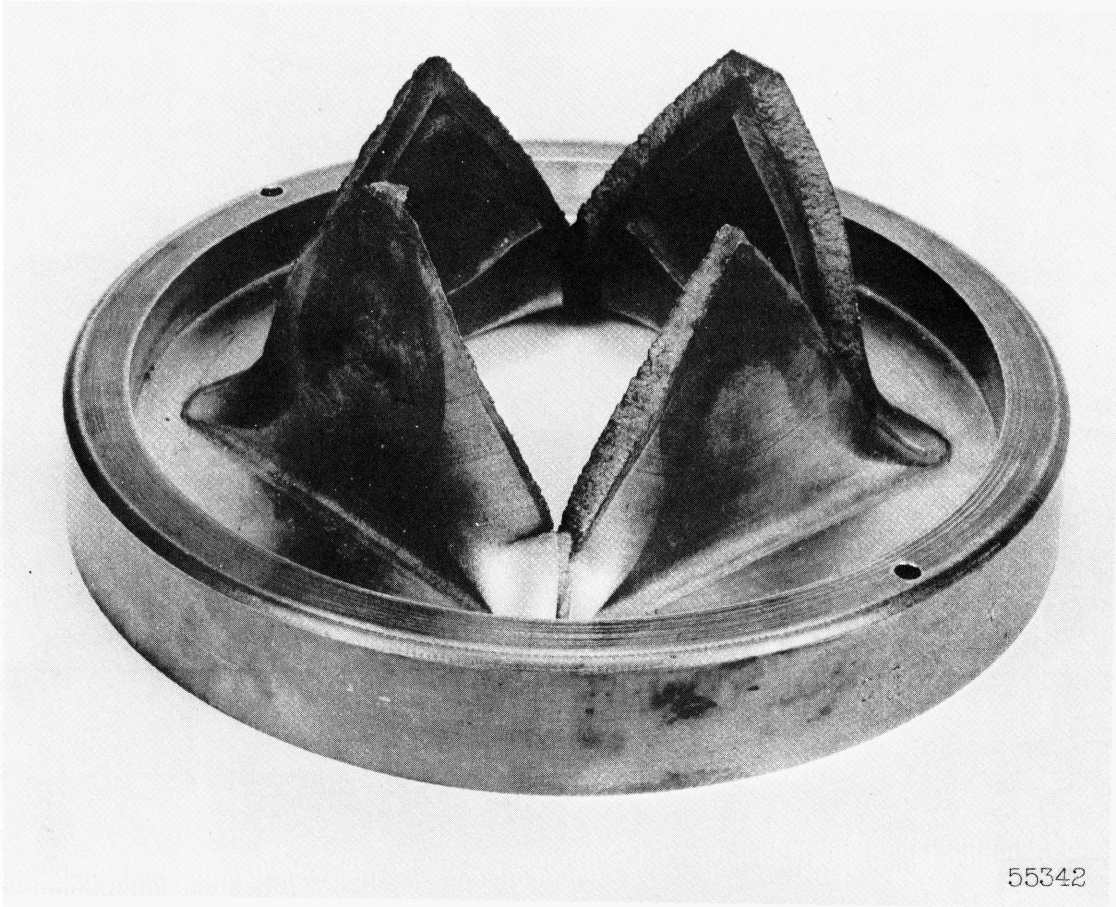


Figure 13 - Petal valve diaphragm with 22° control lines

(UNCLASSIFIED TITLE)

HYPERVELOCITY KILL MECHANISMS PROGRAM

ARPA Order 149-60

Aerothermal Phase

Quarterly Progress Report
For Period Ending
20 June 1963

19 July 1963

T. J. O'Connor
R. Shaw
H. E. Hoercher
R. S. Timmins

RESEARCH AND ADVANCED DEVELOPMENT DIVISION
AVCO CORPORATION
Wilmington, Massachusetts

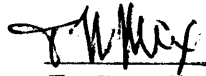
Project Code No. 7300

Contract NOnr 3307(00)

STATUS REPORT

RAD SR 63-134

APPROVED



T. W. Mix
Project Director

This document contains information affecting the National Defense of the United States within the meaning of the Espionage Laws, Title 18, U.S.C., Sections 793 and 794, the transmission or revelation of which in any manner to an unauthorized person is prohibited by law.

C1

(NOT USED)

CONTENTS

II. Aerothermal Phase	C9
A. Experimental	C9
B. Analytical	C15
C. References	C17

ILLUSTRATIONS

Figure 1	Model, Hemisphere-Cone Cylinder Reentry Vehicle	C19
2	Hemisphere-Cone Section	C20
3	Stagnation-Pressure to Pipe-Pressure Ratio as a Function of Pipe-to-Box Pressure Ratio for an Underexpanded Jet Impinging on a Hemisphere	C21
4	Stagnation Point Heat-Transfer Correlation as a Function of Jet Reynolds Number	C22
5	Heat-Transfer Variation on Hemisphere as a Function of Pipe-to-Box Pressure Ratio	C23

TABLES

Table 1	Calorimeter Locations for Hemisphere-Cone Cylinder Model	C24
2	Calorimeter Locations for Hemisphere-Cone Model	C25
3	Test Conditions for Hydrogen-Oxygen Rocket Engine Experiments	C25
4	Test Conditions for 10-Mw Air Arc Experiments	C26
5	Results for Hydrogen-Oxygen Rocket Engine Tests, Hemisphere-Cone-Cylinder Model	C27
6	Results for Hydrogen-Oxygen Rocket Engine Tests, Hemisphere-Cone Model	C29
7	Results for 10-Mw Air Arc Experiments	C32

SYMBOLS

C_d	Discharge coefficient given in reference (5)
d	Diameter of jet orifice
H	Enthalpy, Btu/lb
L	Distance from jet inlet to hemisphere, inches
M	Mach number at the hemisphere
m_{ideal}	Ideal mass flow rate (subsonic compressible or choked) lb/sec
P	Pressure, lb/in. ²
\dot{q}	Heat flux, Btu/ft ² -sec
R	Gas constant, lb-ft/°R/lb _m
r	Distance along surface from stagnation point, feet
T	Temperature, °R
U	Velocity of external flow; velocity of jet at body, ft/sec
γ	Ratio of specific heats
ρ	Density, lb/ft ³
μ	Viscosity, lb/ft-sec

Subscripts

e	external flow
j	jet conditions
o	stagnation conditions
w	wall condition

(NOT USED)

SUMMARY

Experimentally determined heat fluxes experienced by an apparatus designed to simulate a punctured reentry vehicle are presented. The facilities employed as sources of high-enthalpy gas for these experiments were the Avco RAD hydrogen-oxygen rocket engine and the Ten Megawatt (10-Mw) air arc. A correlation of jet impingement heat-transfer ratios is also presented.

(NOT USED)

II. AEROTHERMAL PHASE

A. EXPERIMENTAL

1. Apparatus and Procedure

The apparatus used in the experimental studies of internal heating of a punctured reentry vehicle was designed to simulate two generic families of reentry vehicles: (a) hemisphere-cone-cylinder-flare vehicles with integrated or nonintegrated internal structures, and (b) hemisphere-cone vehicles.

The hemisphere-cone portion of the apparatus, employed in studying internal heat transfer for both families, was machined from OFHC (oxygen-free, high-carbon content) copper. The hemisphere had an internal diameter of 4.0 inches and was tangent to the conical portion of this section. The half-angle of the conical section was 22.5 degrees and it had a base diameter of 10.25 inches. At the base of the cone there was a short cylindrical section with a length of 0.50 inch; this section was instrumented with six insulated copper calorimeters in a common plane, as indicated in figure 1.

All calorimeter front faces are flush with the inner surface of the section. The axes of the calorimeters closest to the base plane of the cone are at an angle of 22.5 degrees from this plane. The extension of the centerlines of these two calorimeters intersects the axis of symmetry of this section in the plane of the base of the cone. The location of each calorimeter in this section is given in table 1.

The cylindrical portion of the apparatus was constructed from standard stainless-steel pipe. The outer cylinder had a length of 16.0 inches and an internal diameter of 10.25 inches. This section was instrumented with five insulated copper calorimeters and two pressure taps, as indicated in figure 1. The location of each calorimeter is given in table 1.

The case of a vehicle of the hemisphere-cone-cylinder-flare configuration with a nonintegrated internal body was simulated by enclosing a cylindrical body with a hemispherical front face within the apparatus. This assembly was aligned so that its axis of symmetry coincided with that of the outer cylinder. The cylindrical section of this assembly had an outside diameter of 6.625 inches and was 16.50 inches in length. It was instrumented with three calorimeters as indicated in figure 1. The location of each calorimeter is given in table 1. The hemispherical front face of the assembly was machined from OFHC copper and had a diameter of 6.562 inches. It was instrumented with three calorimeters, as given in table 1.

The entire apparatus has been sealed from the environment by welding a plate to the rear of the inner body assembly. A section of the entire assembly can be found in figure 1.

The hemisphere-cone section of this apparatus (see figure 2) was employed in the study of internal heating of vehicles of the second generic family. This was accomplished by sealing the rear of this section with a circular flat plate instrumented with six insulated copper calorimeters. Calorimeter locations were at the center of the plate and at radial distances of 1.0, 2.0 (two calorimeters), 3.0 and 4.0 inches. In addition, the plate was provided with five pressure taps at radial distances of 0.875, 1.875, 2.875 (two taps) and 4.875 inches from the center. Calorimeter locations are tabulated in table 2.

Two large threaded holes were cut in the base of each generic model to provide a means of venting the apparatus; vent area on each apparatus was varied by inserting plugs with various hole diameters into two large threaded holes. The vents were positioned so that flow within the apparatus would be symmetrical in nature. With this system, vent diameters could be varied from 0.1875 to 1.05 inches.

A series of experiments was conducted with the previously described hemisphere-cone-cylinder apparatus using the Avco RAD hydrogen-oxygen rocket engine facility as a source of high-enthalpy gas. These experiments were performed with an inlet hole diameter of 0.750 inches located on the axis of symmetry of the apparatus, simulating a puncture at the stagnation point of the reentry vehicle.

The apparatus was coupled directly to the rocket engine facility at a point between the combustion chamber and the exit nozzle, as described above. The passage from the rocket engine and the apparatus was sealed with a gasket, acting as a rupture diaphragm, as indicated in figure 1.

The procedure followed in conducting each test is presented here. Prior to each test, the enclosed volume of the model was purged with argon to remove any residual hydrogen and oxygen from the system. This precaution was necessary to eliminate any combustible gas mixture from the model. The rocket engine was preloaded with hydrogen and oxygen to obtain the desired stagnation pressure and combustion gas composition. The engine was then ignited and brought to stable operating conditions, using a quick start procedure (i. e., chamber pressure and combustion would become stable in less than 0.50 second). During this rapid transition to stable operating conditions, the diaphragm between the apparatus and the rocket engine ruptured allowing the high-enthalpy combustion products to enter the apparatus.

In the experiments with the 0.75-inch diameter hole, data acquisition system limitations made it necessary to restrict instrumentation to nine channels. Pressures recorded during each test were chamber pressure, box pressure, hydrogen and oxygen line pressures, and the pressure in the pipe directly opposite the passage into the apparatus. Hence the number of calorimeters employed in each test was a maximum of four. Due to interest in the high heating rates experienced in the vicinity of the impingement point of the jet, the thermocouple outputs recorded were those at stations 4, 15, 16 and 17 (see table 1 for calorimeter locations). Test conditions for these experiments are presented in table 3.

A limited number of tests were conducted with the hemisphere-cone model on the rocket engine facility with a 0.50-inch diameter inlet hole. Experiments were conducted with the system vented and unvented. In the unvented firings the response time of the system proved to be so short that little or no heating was experienced. Vented tests were conducted with vent-to-inlet area ratios of 0.945 and 3.78. Heat fluxes were measured at all calorimeter locations and at positions 1 and 4 on the conical portion of the model and at all calorimeter stations on the rear plate. The internal pressure was measured at a radial distance of 0.875 inches from the center of the back plate. Test conditions for these experiments can be found in table 3.

Attempts were made to measure the gas temperature within the apparatus in several of the previously cited experiments. However conduction losses experienced in these measurements were found to be so large that the thermocouple output measured was unreliable.

Ten Megawatt (10-Mw) Arc Tests

A number of tests were conducted with the hemisphere-cone-cylinder model (figure 1) with a 0.50-inch diameter inlet hole on the Avco 10-Mw Air Arc Facility. All tests considered in this report were performed on an unvented system.

The essential components of the 10-Mw multi-arc heat, include a 4-inch diameter plenum chamber into which four 2-Mw plasma generators exhaust radially and one exhausts axially. The arc-heated air mixes in the plenum chamber and exhausts axially in the sixth direction. The high-enthalpy air passes through a water-cooled transition section having a length of 3.0 inches and then through a 10-inch water cooled extension. Downstream of the extension was an uncooled copper tube 9.81 inches in length; after passing through the uncooled section the high-enthalpy air flows through a sonic nozzle and exhausts into the atmosphere. A passage

with an inside diameter of 0.50 inches was provided for gas flow from the uncooled pipe into the test apparatus. This passage opens into the uncooled copper section at a right angle to the main gas flow. The centerline of the passage was located at a distance of 6.75 inches from the upstream of the uncooled pipe. The passage was a total distance of 19.75 inches from the plenum chamber. The inside diameter of all pieces between the plenum chamber and the exit nozzle was 1.25 inches.

The actual procedure employed in the experimental tests is described here. Arc operating conditions (i. e., gas flow rates, exhaust nozzle diameter, and power to each arc) which were required to obtain a desired plenum pressure and gas enthalpy were determined from arc data recorded in previous experiments. Prior to firing the arc, gas flow rate through the system was adjusted to the desired value and recorded. After gas flow stabilization, the power breaker was closed. The arcs between the carbon cathodes and water-cooled copper anodes were initiated by means of a tungsten wire strung through holes in the cathode and contacting the anode. The air was injected tangentially into each arc chamber and was heated to a high temperature by passing through the swirling arc. Steady-state values of arc current, voltage and plenum pressure were obtained in approximately 1 second after the start of the experiment. Steady state operating conditions for these experiments are tabulated in table 4.

As was the case in the unvented experiments on the rocket engine facility, a gasket was placed across the passage between the model and the main gas flow. The sudden rise in plenum pressure which occurred when the arc was fired caused the diaphragm to rupture allowing high-enthalpy air to flow into the apparatus.

2. Experimental Results

a. Hydrogen-Oxygen Rocket Engine Experiments

Experimental heat fluxes obtained in the tests conducted on the rocket engine facility with the vented hemisphere-cone-cylinder apparatus were similar in nature to those reported in reference 1 for the 0.50-inch diameter inlet hole. In general the response of the apparatus was more rapid with the 0.75-inch diameter inlet hole and heating was more severe at given values of pipe and box pressure. For example, at a chamber pressure of approximately 85 psia and a box pressure of 55 psia, the measured heat flux at the apex of the inner body was 275 Btu/ft²-sec and 600 Btu/ft²-sec for inlet hole diameters of 0.50 and 0.75 inch, respectively. With

a fixed distance of the calorimeter from the origin of jet, increasing the jet diameter resulted in a decreased jet-length-to-diameter ratio. Hence, the attenuation of both jet velocity and enthalpy was less pronounced with the larger hole, and jet impingement heating was more severe.

As was the case for the smaller hole, the stagnation point heat flux rose to a peak value very early in each experiment and then decreased to a relatively constant value for times longer than 1.5 seconds after the start of the test. Heating conditions at the three other stations monitored in these experiments remained relatively constant with time after the initial transient. The maximum heat flux experienced in these firings was 1275 Btu/ft²-sec at a chamber and box pressure of 123.2 psia and 22.7 psia, respectively. Experimental heat fluxes for all tests conducted with the 0.75-inch diameter inlet hole are tabulated in table 5.

The measured pressure within the system exhibited a very sharp peak very early in each test. Following this, the pressure decreased to a relatively low value in a time of less than 1.5 seconds. The internal pressure history had a brief transition period following this local minimum and then increased gradually for the remainder of the test period.

Internal heat-transfer rates were obtained from experiments on the hydrogen-oxygen rocket engine facility with the hemisphere-cone model described in section A.1. The system was instrumented with eight transient copper calorimeters as cited previously. Pressures recorded continuously during each firing were: chamber pressure, pipe pressure, oxygen-and hydrogen-line pressures and box pressure. The pressure within the apparatus was measured at a point 0.875 inches from the center of the rear plate.

Since it was found that there was little or no response in the system when the apparatus was run in an unvented condition,² all experiments were with a vented model. Vent-to-inlet area ratios were 0.945 and 3.78; the inlet hole had a diameter of 0.50 inch.

Computed heat fluxes obtained from the experimental data in these tests were considerably lower than those experienced under comparable operating conditions (i. e., chamber pressure, internal pressure, and inlet-hole diameter) with the hemisphere-cone-cylinder apparatus. Once again this variation in heat flux at the impingement point was attributed to the attenuation of jet velocity and enthalpy in the distance from the inlet hole to the calorimeter. In these experiments, the impingement point was a distance of

19.3 diameters downstream of the jet exit plane while in the other model the maximum distance was 11.7 diameters with a 0.50-inch inlet hole.

In general there was little variation in the measured heat flux with radial distance on the instrumented rear plate of the apparatus (e. g., the flux at a radial distance of 4.0 inches was never less than 50 percent of that experienced on the center of the plate). The response of the system following breaking of the rupture diaphragm was much the same as that noted in reference 1 for the hemisphere-cone-cylinder model. Computed heat flux for all stations on the rear plate peaked very early in each experiment and then dropped off fairly rapidly with time. Later in the test, heating rates approached a steady state value or decreased very slowly with time. An example of the above flux history is as follows: for an experiment with an average chamber pressure of 107 psig, experimental heat fluxes at station A (see table 2 for calorimeter location) were computed as 260, 152, 155 and 160 Btu/ft²-sec at times of 0.50, 2.00, 4.00 and 5.00 seconds, respectively.

Pressures recorded within the apparatus during the experiments had the same variations with time as described in previous reports^{1, 2, 3} concerning vented tests. The internal pressures had a very pronounced peak early in time and then dropped off rapidly with time. Following a local minimum in the internal pressure, the pressure increased slowly with time for the remainder of the experiment. Experimental results for all tests conducted with the hemisphere-cone model are tabulated in table 6.

b. 10-Mw Unvented Experiments

In conjunction with the vented tests conducted on this facility, described in reference 2, several unvented experiments were performed with the hemisphere-cone-cylinder model.

The response of the system following the breaking of the rupture diaphragm was similar to that reported in reference 3 for unvented experiments conducted in the hydrogen-oxygen rocket engine facility. Internal and external pressures equalized in a short period of time. In all cases, heat fluxes obtained at the various stations in the forward portion of the apparatus reached a peak value very early in time and then decreased for the remainder of the experiment. The initial peak values occurred at a time when the pipe and box pressures were not equal, i. e., the high-enthalpy air entering the apparatus was in the form of a high-velocity jet. At later times the heat fluxes were of lower magnitude, and flow

into the apparatus was dependent on energy and material balance considerations. As in all experiments conducted to date, the more severe heating conditions were experienced in the vicinity of the jet-impingement point. Heat fluxes recorded by calorimeters in the conical portion of the apparatus were always of greater magnitude than those measured in the cylindrical section. This phenomenon was a result of gas temperatures and recirculation in those portions of the apparatus which surround the jet of high-enthalpy gas.

Experimental results obtained in all unvented tests conducted on the 10-Mw facility are presented in table 7. Experimental pressure data from two tests (3553 and 3561) are questionable due to an apparent shift in the zero point of the transducers employed in the firings. In some experiments poor resolution of the traces obtained for several calorimeter stations indicated that there was little or no response during the tests. Data for these stations are indicated by dashed lines in table 7.

B. ANALYSIS

1. Stagnation Point Heating

Several attempts were made to correlate the stagnation-point heat fluxes from the two sets of rocket motor tests (HD = 7.8, L/D = 11.7) and the air arc tests. All approaches made use of the Fay and Riddell stagnation-point heating expression:

$$\dot{q} \propto \left[\frac{(\rho\mu)_w}{(\rho\mu)_e} \right]^n \sqrt{(\rho\mu)_e \frac{dU}{dr}} (H_e - H_w).$$

The flow conditions at the stagnation point of the hemisphere were calculated by a variety of procedures. An outline of these methods is as follows:

a. The underexpanded jets were assumed to expand to the isentropic Mach number at an imaginary distance and equivalent diameter given by Love and Rousso in reference 4. The jet was then assumed to diffuse according to Warren's theory with $T_{oi}/T_a = 2.0$ (ratio of initial jet-stagnation temperature to ambient temperature). If the computed Mach number at the hemisphere was greater than 1.0, a normal shock was assumed and ideal gas relations were employed to compute the flow properties at the stagnation point. The velocity gradient was then assumed independent of pressure ratio and proportional to the calculated velocity of the jet at the hemisphere divided by the orifice diameter. The enthalpy decay of the jet was assumed similar to the total temperature decay given by Warren.⁴ With this approximation the enthalpy at the wall could be estimated.

b. The underexpanded jets were assumed to expand to the isentropic Mach number and area ratio. A normal shock was then assumed to occur at one-half the shock node distance, and the conditions following the shock were used to initiate a jet decay as given by Warren.⁴ The enthalpy decay and velocity gradient were approximated as described in method (a.).

c. Measurements of the stagnation pressure indicated that the procedures used in methods (a.) and (b.) falsely predicted the stagnation pressure at large pressure ratios. To improve the correlation, the stagnation pressure was taken from the correlation shown in figure 3. The jet Mach number used to compute the velocity gradient was taken as the Mach number indicated by the static-to-stagnation pressure ratio for $\gamma = 1.23$. The enthalpy attenuation was computed as described in method (a.).

d. The results of the above attempts at correlation indicated that the heating was more strongly a function of the pipe pressure and the L/D ratio than was predicted by Warren's theory. The pressure ratio influence indicated a jet Reynolds number effect, and the L/D influence indicated the enthalpy attenuation of severely underexpanded jets could not be adequately predicted by Warren's theory in light of this evidence so the data was correlated by an equation of form:

$$\dot{q} = K (Re_j)^n \left[\frac{(\rho\mu)_w}{(\rho\mu)_e} \right]^m \sqrt{(\rho\mu)_e \frac{dU}{dr} \left(\frac{d}{L} \right)} (H_o - H_w) \quad (1)$$

Equation 1 will correlate all the data to within 20 percent in $n = 1.0$, $m = 0.2$ and $K = 1.29 \times 10^{-4}$. The steady state values of all tests are shown in figure 3. The transients from 1.0 second to the end of each test fall in the same band but have been omitted for clarity.

The various factors in equation 1 were approximated as follows:

$$1) \quad Re_j \equiv \left(\frac{\rho U d}{\mu} \right)_j = \left[\frac{4 C_d \dot{m}_{ideal}}{\pi \mu d} \right]$$

2) H_o = unattenuated enthalpy of the gas in the pipe.

$$3) \quad \sqrt{(\rho\mu)_e \frac{dU}{dr}} \approx \sqrt{\left(\frac{P_o}{RT_o} \right) \mu_e \frac{U}{d}} .$$

where

$$U = M \sqrt{\left(\frac{2\gamma}{\gamma+1}\right) g R T_o}$$

$$\mu_e = K \sqrt{T_o}$$

therefore

$$\sqrt{\rho \mu_e \frac{dU}{dr}} = \sqrt{\frac{P_o M}{d}} \left\{ K \left[\frac{2 \gamma g}{R (\gamma + 1)} \right]^{1/2} \right\}^{1/2}$$

Although equation 1 has only been applied to a limited range of L/D and Re_j , it is the best correlation found thus far. When more is known as to the structure and enthalpy decay of hot underexpanded jets, a more sophisticated approach may be possible.

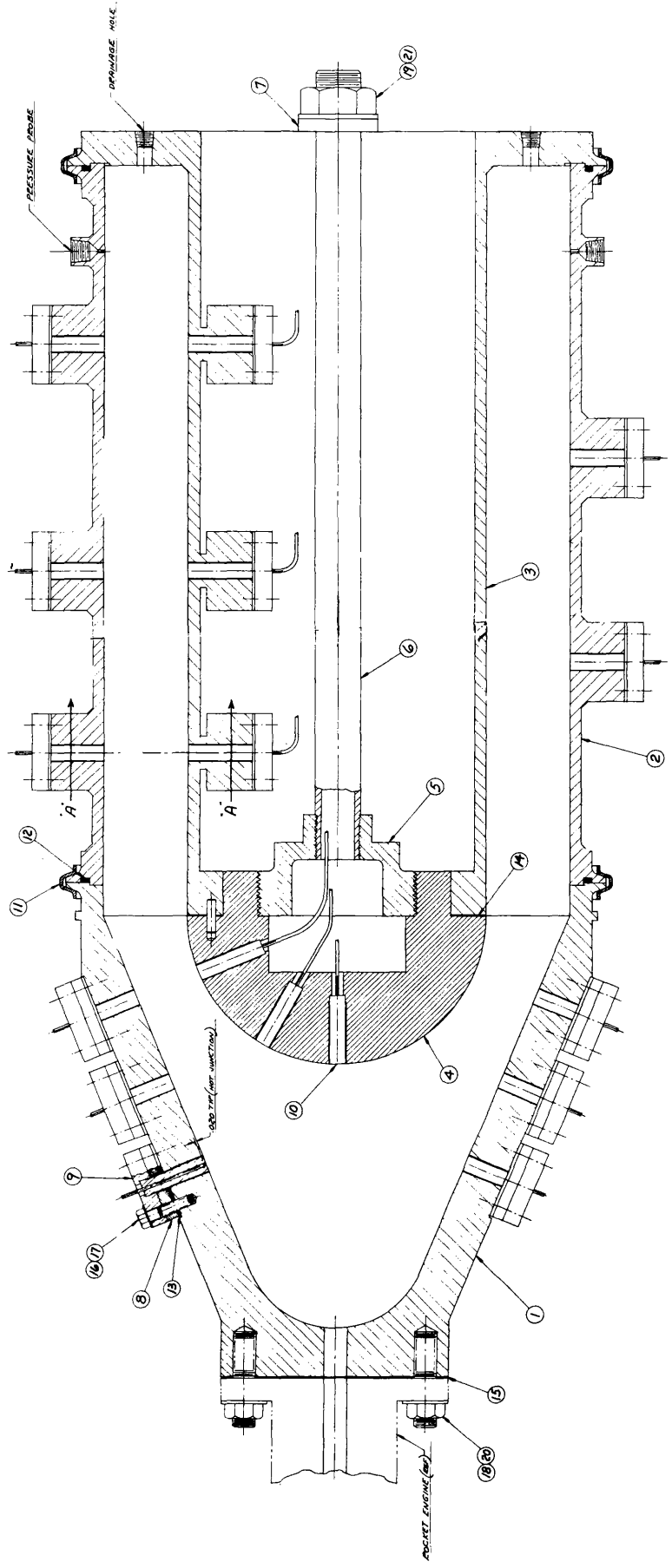
2. Off-Stagnation Point Heating

The heat fluxes at two locations off the stagnation point may be related to the stagnation heat flux as seen in figure 5. The heat-flux ratio at 30 degrees (1.72-in. arc length) shows a transition at pressure ratio between 3 and 4. This is the range of pressure ratio when a normal shock appears in the jet and the first cell in the series of shocks becomes stable. As a result of this structure the jet spreading angle becomes smaller, thus the stagnation heat flux is increased relative to the locations off the stagnation point. The location at 67 degrees (3.88-inch arc length) shows just a gradual decrease relative to the stagnation point. Since this location is more than 7 jet diameters away from the stagnation point, the change in jet structure apparently has little effect on heat flux at this position.

C. REFERENCES

1. Hoercher, H. E., T. J. O'Connor, and R. S. Timmins, Hypervelocity Kill Mechanisms Program, Avco RAD SR-63-9 (18 January 1963). Secret
2. O'Connor, T. J., H. E. Hoercher, R. Shaw, and R. S. Timmins, Hypervelocity Kill Mechanisms Program, Avco RAD SR-63-121 (21 June 1963). Secret
3. Hoercher, H. E., T. J. O'Connor, and R. S. Timmins, Hypervelocity Kill Mechanisms Program, Avco RAD SR-62-200 (24 October 1962). Secret

4. General Electric Company, MSVD, Hypervelocity Kill Mechanisms Feasibility Study, Internal Heating, Document No. 62SD560 (20 May 1962). Secret
5. Callaghan, E. E. and D. T. Bowden, Investigation of Flow Coefficient of Circular, Square, and Elliptical Orifices at High Pressure Ratios, NACA TN 1947.



(G) ASSEMBLY

NOTE: SCRIBE MARK ON MATING PLANES SO THAT ALL CASIMETERS ARE ON SAME PLANE (A) AT ASSY.

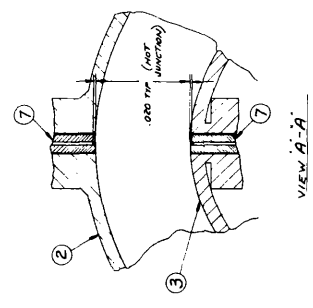


Figure 1 MODEL, HEMISPHERE-CONE-CYLINDER REENTRY VEHICLE

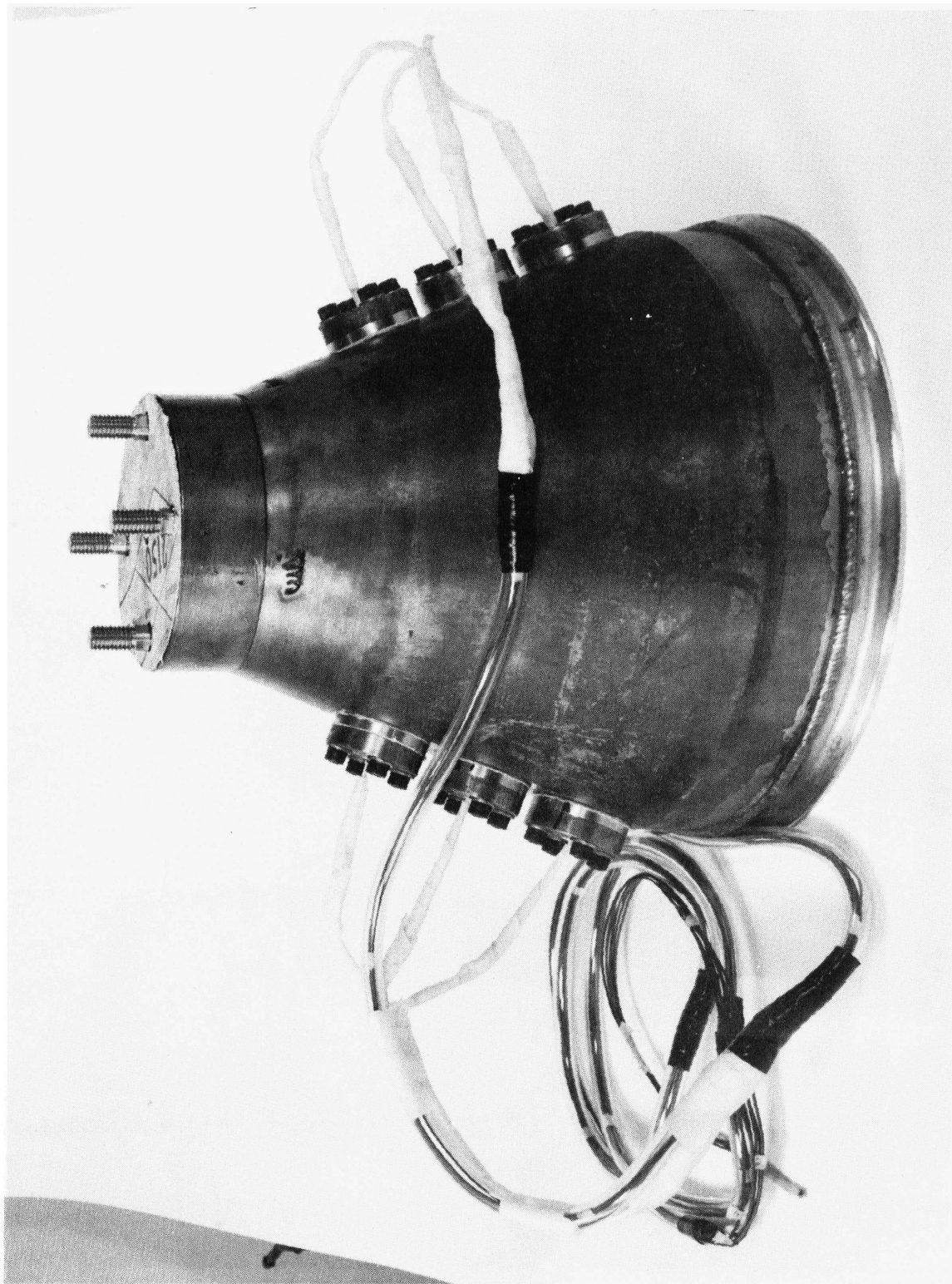


Figure 2 HEMISPHERE-CONE SECTION
P-8384F

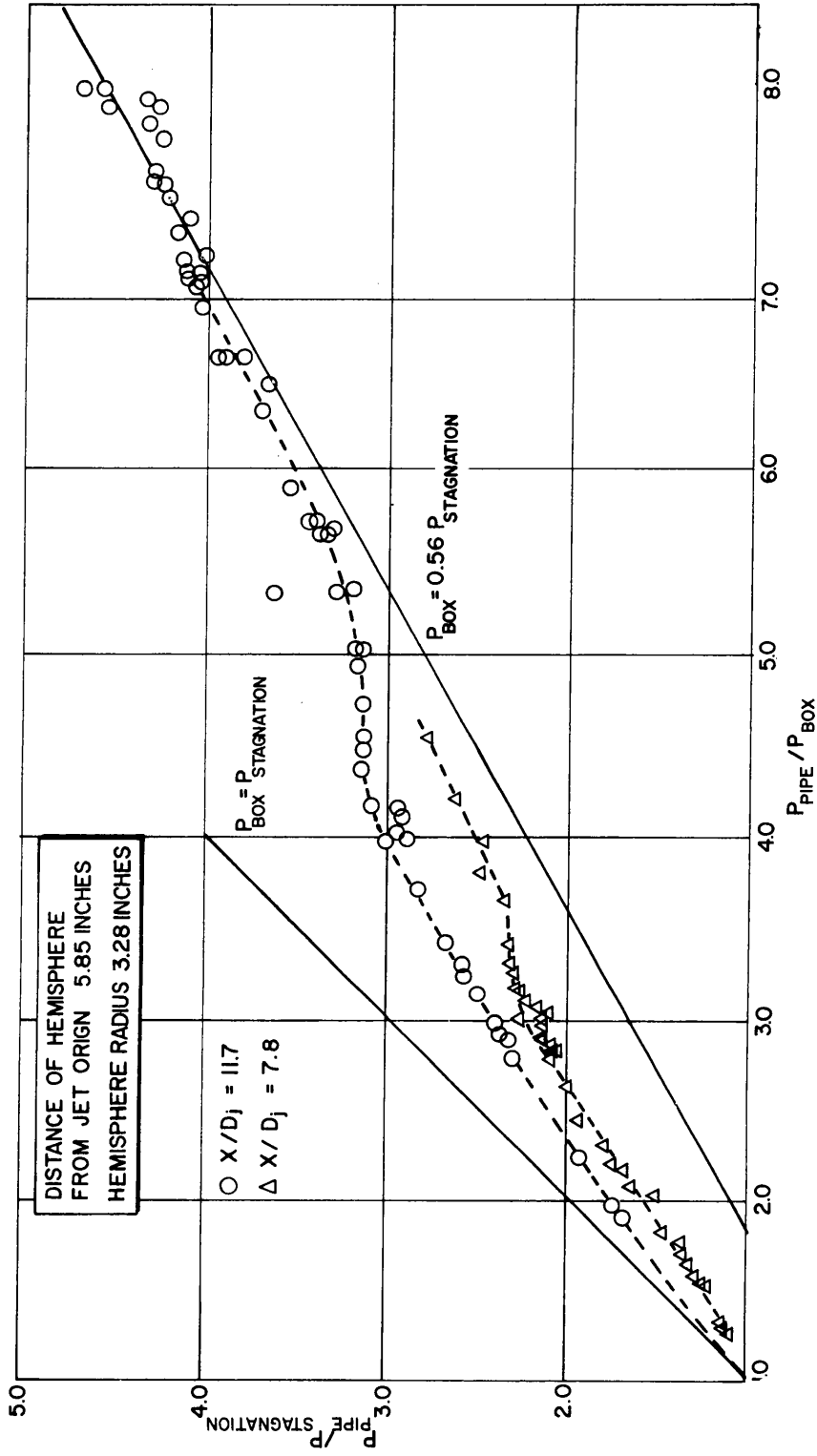


Figure 3 STAGNATION-PRESSURE TO PIPE-PRESSURE RATIO AS A FUNCTION OF PIPE-TO-BOX PRESSURE RATIO FOR AN UNDEREXPANDED JET IMPINGING ON A HEMISPHERE
 63-5716

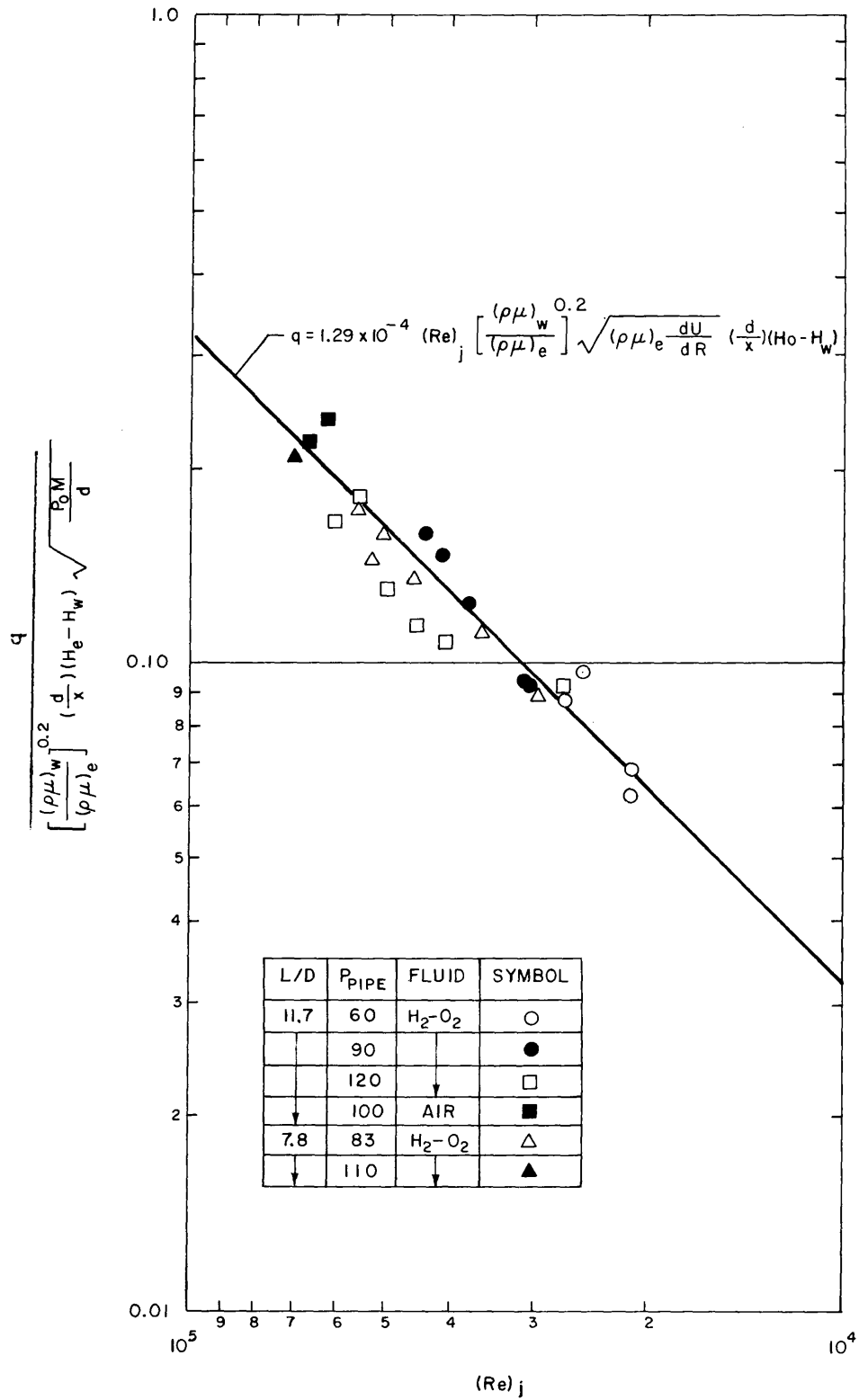


Figure 4 STAGNATION POINT HEAT-TRANSFER CORRELATION AS A FUNCTION OF JET REYNOLDS NUMBER
63-6522

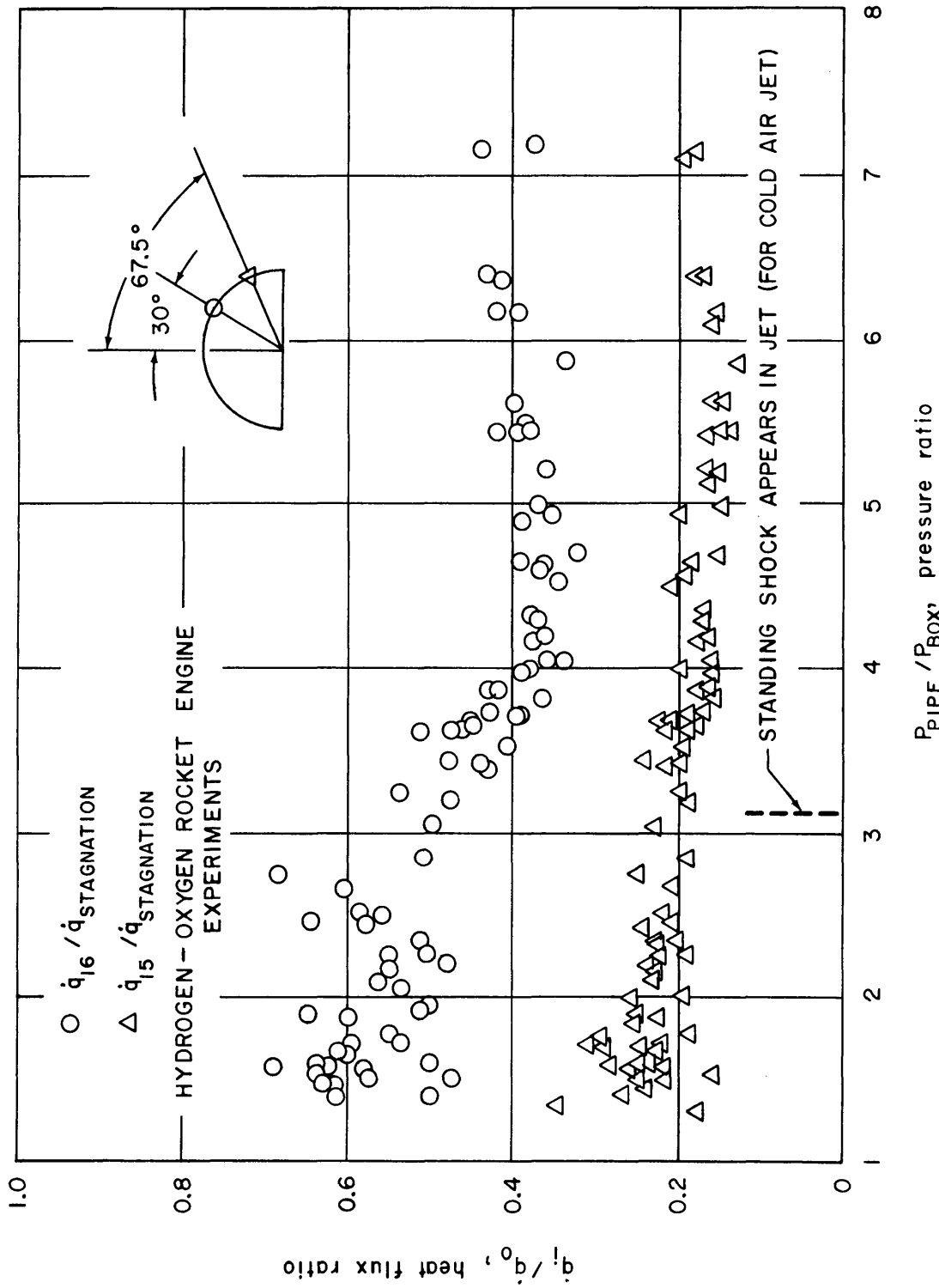


Figure 5 HEAT-TRANSFER VARIATION ON HEMISPHERE AS A FUNCTION OF PIPE-TO-BOX PRESSURE RATIO
63-6523

TABLE 1

CALORIMETER LOCATIONS FOR AGGRAVATION EXPERIMENTS

Number	Portion of Model	Location
*TC 1	Cone	Axis of calorimeter 22.50 degrees from cone base with apex of angle at center of hemispherical cap.
TC 2	Cone	2.0 inches from calorimeter 1.
TC 3	Cone	2.0 inches from calorimeter 2.
TC 4	Cone	180 degrees around model axis from calorimeter 1.
TC 5	Cone	180 degrees around model axis from calorimeter 2.
TC 6	Cone	180 degrees around model axis from calorimeter 3.
TC 7	Outer Cylinder	5.50 inches from base of cone.
TC 8	Outer Cylinder	10.0 inches from base of cone, coplanar with 7.
TC 9	Outer Cylinder	12.5 inches from base of cone, 180 degrees around model axis from calorimeters 7 and 8.
TC 10	Outer Cylinder	7.5 inches from base of cone, coplanar with calorimeter 9.
TC 11	Outer Cylinder	3.5 inches from base of cone, coplanar with calorimeter 9.
TC 12	Inner Cylinder	3.42 inches from base of cone.
TC 13	Inner Cylinder	7.42 inches from base of cone, coplanar with 12.
TC 14	Inner Cylinder	12.42 inches from base of cone, coplanar with 12.
TC 15	Hemispherical Cap	Angle between calorimeter and model center-lines: 67.50 degrees.
TC 16	Hemispherical Cap	Angle between calorimeter and model center-lines: 30.0 degrees.
TC 17	Hemispherical Cap	Angle between calorimeter and model center-lines: 0 degrees.

All calorimeters are 0.375 inch in diameter and 1.50 inches long.

*TC = Thermocouple.

TABLE 2

CALORIMETER LOCATIONS FOR HEMISPHERE-CONE MODEL

Station	Radial Distance (inches)	Location*
A	0.0	Center of rear plate.
B	1.0	1-inch from station A.
C	2.0	90 degrees from radius through station B.
D	2.0	On diameter through stations A and B, 180 degrees away from station B.
E	3.0	On radius from A to B.
F	4.0	On radius from A through D.

* Calorimeter stations 1 and 4 are identical to those cited in table 1.

TABLE 3

TEST CONDITIONS FOR HYDROGEN-OXYGEN ROCKET ENGINE EXPERIMENTS

Experiment Number	Chamber Pressure (psia)	Mixture Ratio (1bO ₂ /1bH ₂)	Stagnation Temperature (°R)	Stagnation† Enthalpy (Btu/lb)	Inlet Diameter (inches)	Vent-to Inlet-Area Ratio
42*	85.2	4.05	5425	5170	0.750	0.222
43*	82.7	4.07	5440	5180	0.750	0.420
44*	82.2	4.08	5440	5180	0.750	0.890
45*	82.2	4.20	5465	5213	0.750	1.680
46*	80.7	3.80	5360	5100	0.750	1.680
47*	111.7	3.96	5400	5137	0.750	1.680
48*	81.2	3.80	5360	5100	0.750	3.240
49	63.7	3.70	5210	5030	0.500	3.78
50	90.2	4.52	5730	5290	0.500	3.78
51	120.7	4.08	5460	5180	0.500	3.78
52	90.2	3.70	5280	5030	0.500	3.78
53	91.2	3.92	5370	5160	0.500	0.945
54	121.7	4.09	5420	5175	0.500	0.945
55	90.7	3.88	5370	5140	0.500	0.945
56	63.7	3.70	5280	5030	0.500	0.945

* Conducted with hemisphere-cone-cylinder model; all other experiments performed with hemisphere-cone model.

† Enthalpy computed assuming complete combustion of all O₂ to H₂O. Base for computation H₂O(g) and H₂(g) at 298°K.

TABLE 4

TEST CONDITIONS FOR 10-MW AIR ARC EXPERIMENTS

Run Number	Plenum Pressure, (atmosphere)	Nozzle Diameter (inches)	Power to Air (Mw)	Mass Flow Rate (lb sec)	Enthalpy* (Btu/lb)	Inlet Hole Diameter (inches)
3353	6.29	0.825	0.887	0.276	3020	0.50
3557	3.71	1.200	2.261	0.217	9700	0.50
3559	10.44	0.60	0.766	0.241	3020	0.50
3561	8.98	0.60	0.626	0.214	2760	0.50

* Computed from mass flow rate and nozzle size.

TABLE 5

TEST RESULTS FOR HYDROGEN-OXYGEN ROCKET ENGINE TESTS,
HEMISPHERE-CONE-CYLINDER MODEL

<u>Test No. 42</u>						
Time (seconds)	P _{pipe} (psig)	P _{box} (psig)	Station			
			14	15	16	17
(Heat Flux, Btu/ft ² -sec)						
0.0	86.2	0.0	0.0	0.0	0.0	0.0
0.2	75.5	39.0	85	118	245	435
0.5	76.5	68.5	20	62	102	195
0.8	71.2	58.2	112	160	340	520
1.0	70.0	54.5	120	185	335	575
1.5	68.5	50.5	115	196	288	572
2.0	68.5	52.5	100	193	261	532
3.0	70.6	56.2	110	165	255	460
4.0	71.5	62.0	98	125	231	400
5.0	72.0	63.5	94	107	205	355
<u>Test No. 43</u>						
0.0	87.5	0.7	0.0	0.0	0.0	0.0
0.3	76.0	45.5	40.0	15	125	207
0.5	71.5	39.0	105	95	210	377
1.0	67.5	26.5	136	150	300	707
1.1	67.0	28.2	126	163	317	755
2.0	67.4	40.7	117	141	290	605
3.0	68.3	46.7	111	142	277	545
4.0	69.5	51.0	107	125	265	490
4.2	69.2	50.2	102	122	260	487
<u>Test No. 44</u>						
0.0	88.0	0.7	0.0	0.0	0.0	0.0
0.2	76.0	28.3	92.0	53.0	135	242
0.5	69.6	9.8	112	112	242	602
0.7	68.0	10.8	105	126	242	657
1.0	68.0	14.0	105	105	223	550
1.5	67.3	17.5	116	117	248	542
2.0	67.2	22.3	115	135	275	578
3.0	66.6	27.5	105	145	292	585
3.8	67.2	29.0	98	137	298	612

TABLE 5 (Concl'd)

<u>Test No. 45</u>						
Time (seconds)	P _{pipe} (psig)	P _{box} (psig)	Station			
			14	15	16	17
			(Heat Flux, Btu/ft ² -sec)			
0.0	87.8	0.0	0.0	0.0	0.0	0.0
0.2	80.8	10.2	98	78	178	373
0.5	69.3	2.7	95	135	252	722
1.0	67.5	5.5	105	125	235	597
1.5	66.6	7.3	110	127	254	571
2.0	67.3	8.8	112	142	275	572
2.1	67.3	8.4	110	137	271	547
2.3	60.5	9.0	117	147	300	601
<u>Test No. 46</u>						
0.0	86.0	0.0	0.0	0.0	0.0	0.0
0.2	74.7	14.2	100	105	260	411
0.5	67.0	1.4	105	180	265	752
0.6	67.0	2.8	108	176	260	777
1.0	66.0	3.8	112	142	225	650
2.0	65.7	7.2	117	127	270	615
3.0	65.1	9.0	110	110	270	565
3.8	65.6	10.9	103	93	260	565
<u>Test No. 47</u>						
0.0	126.0	0.0	0.0	0.0	0.0	0.0
0.1	107.0	21.2	150.0	80.0	228	315
0.2	102.0	15.5	165.0	125	315	675
0.4	98.0	8.0	178.0	238	450	1275
1.0	97.0	15.8	180.0	195	400	880
1.5	96.5	19.1	158.0	196	408	850
2.0	96.0	21.0	160.0	185	415	812
2.5	96.8	21.2	170.0	195	440	840
2.8	96.5	22.2	180.0	200	462	855
<u>Test No. 48</u>						
0.0	87.0	0.0	0.0	0.0	0.0	0.0
0.1	75.5	9.8	45	20	45	215
0.3	70.0	1.0	92	80	190	635
0.8	67.0	1.0	120	55	270	825
1.0	66.3	2.0	106	112	245	704
1.5	66.4	2.0	111	127	250	640
2.0	65.5	3.0	105	135	255	647
2.2	65.5	4.0	100	137	255	627

TABLE 6

RESULTS FOR HYDROGEN-OXYGEN ROCKET ENGINE TESTS,
HEMISPHERE-CONE MODEL

<u>Test No. 49</u>										
Time (seconds)	P _{pipe} (psig)	P _{box} (psig)	Station							
			A	B	C	D	E	F	1	4
(Heat Flux, Btu/ft ² sec)										
0.0	5.0	0.0	0.0	0.0	0.0	0.0	0.0	0.0	0.0	0.0
0.4	50.5	1.5	165	149	113	137	109	72	60	60
1.0	49.6	1.0	146	145	137	147	118	107	69	57
2.0	48.7	1.5	115	116	112	116	106	90	68	60
4.0	48.5	2.4	89	83	82	78	76	73	68	62
6.0	48.5	2.5	77	66	68	62	56	62	62	61
8.0	48.5	2.8	75	66	53	59	46	49	60	55
<u>Test No. 50</u>										
0.1	4.0	0.0	0.0	0.0	0.0	0.0	0.0	0.0	0.0	0.0
0.3	64.0	9.5	169.0	200.0	156.0	246.0	163.0	144.0	100.0	80.0
0.5	77.0	2.0	242.0	238.0	236.0	208.0	148.0	137.0	104.0	75.0
1.0	76.0	3.5	152.0	150.0	142.0	155.0	120.0	104.0	88.0	70.0
2.0	76.0	4.5	130.0	104.0	102.0	104.0	92.0	88.0	77.0	65.0
3.0	76.2	5.5	132.0	122.0	100.0	104.0	82.0	81.0	79.0	70.0
4.0	75.2	5.7	134.0	120.0	97.0	106.0	87.0	88.0	65.0	66.0
5.0	75.0	6.0	135.0	130.0	93.0	101.0	80.0	74.0	69.0	60.0
6.0	75.0	6.5	130.0	134.0	95.0	91.0	68.0	72.0	58.0	58.0
<u>Test No. 51</u>										
0.1	7.5	0.5	0.0	0.0	0.0	0.0	0.0	0.0	0.0	0.0
0.4	105	4.0	220	211	198	237	165	150	98	82
1.0	106	7.8	155	160	146	162	131	112	96	80
2.0	106	9.5	162	145	122	135	112	98	93	79
3.0	106	10.0	170	160	129	135	101	95	83	76
4.0	106	10.5	180	167	128	135	100	94	79	74
5.0	106	11.0	195	182	131	131	100	95	77	71
6.0	107	11.5	185	178	125	125	92	85	71	63

TABLE 6 (Cont'd)

Test No. 52										
Time (seconds)	P _{pipe} (psig)	P _{box} (psig)	Stations							
			A	B	C	D	E	F	1	4
(Heat Flux, Btu/ft ² sec)										
0.2	4.0	0.0	0.0	0.0	0.0	0.0	0.0	0.0	0.0	0.0
0.5	76.5	1.5	186	190	166	195	143	130	96	66
0.6	78.2	1.8	232	206	196	178	140	121	95	75
1.0	75.8	3.1	160	166	144	150	125	95	93	71
2.0	75.2	4.5	132	108	107	106	85	88	80	71
3.0	75.0	5.6	138	114	100	110	78	78	76	65
4.0	75.5	5.6	140	120	97	107	78	74	71	63
5.0	76.2	6.2	149	133	99	104	74	74	67	64
5.8	77.0	6.6	162	130	100	100	65	70	56	62
Test No. 53										
0.0	85.0	0.0	0.0	0.0	0.0	0.0	0.0	0.0	0.0	0.0
0.20	78.3	39.3	172	165	152	134	82	69	72	54
0.30	77.8	28.7	195	163	162	192	118	90	99	70
0.70	76.3	13.5	163	159	163	182	132	118	105	88
1.00	76.2	18.3	170	160	154	154	140	106	100	90
2.00	76.5	26.7	133	125	122	122	111	96	94	87
3.00	76.2	31.2	120	114	103	112	97	93	90	87
4.00	76.7	34.3	126	116	98	110	90	90	84	81
4.20	76.5	34.8	120	114	94	117	85	87	83	78
Test No. 54										
0.0	9.0	0.0	0.0	0.0	0.0	0.0	0.0	0.0	0.0	0.0
0.30	106	37.0	238	240	230	256	---	150	132	90.0
0.50	106	29.0	255	232	241	267	---	170	140	109
1.00	107	37.0	188	193	196	202	---	140	139	120
2.00	107	43.0	153	152	154	156	---	123	121	111
3.00	107	47.0	148	142	131	139	---	116	113	103
4.00	106	49.0	155	155	147	133	---	110	107	105
5.00	107	51.0	158	161	137	142	---	106	100	92
5.60	107	51.0	196	194	162	170	---	122	109	104

TABLE 6 (Concl'd)

Test No. 55										
Time (seconds)	P _{pipe} (psig)	P _{box} (psig)	Stations							
			A	B	C	D	E	F	1	4
(Heat Flux, Btu/ft ² sec)										
0.20	5.0	5.0	0.0	0.0	0.0	0.0	---	0.0	0.0	0.0
0.50	76.2	9.1	220	194	191	186	---	147	113	89
1.0	75.5	16.5	177	174	168	166	---	132	110	103
2.0	76.1	25.0	156	152	152	147	---	117	108	95
3.0	75.5	29.5	135	127	123	123	---	111	110	96
4.0	76.0	32.0	127	116	114	114	---	101	97	96
5.0	75.2	31.8	123	111	100	104	---	94	94	85
6.0	75.5	32.5	139	128	106	118	---	88	86	87
Test No. 56										
0.0	56.5	0.0	0.0	0.0	0.0	0.0	---	0.0	0.0	0.0
0.2	53.0	24.2	81.5	71.0	61.0	94.0	---	49	35	45
0.7	50.0	5.5	143.0	129.0	118.0	129.0	---	96	71	57
1.0	50.5	7.0	123	123.0	118	131.0	---	95	67	73
2.0	49.4	11.7	104	108	106	100	---	77	62	65
4.0	48.8	15.5	93	86	79	79	---	72	66	65
6.0	48.6	19.5	95	79	70	72	---	62	61	66
8.0	49.0	22.7	87	74	62	64	---	50	55	48

DISTRIBUTION

<u>Addressee</u>	<u>Copy No.</u>
Director, U. S. Naval Research Laboratory (Code 1570) Washington 25, D. C.	1-150
Central Files	151
Document Control	152-174
Research Library	175-176

(NOT USED)

DOCUMENT NO. 63SD700

This document contains
Copy number 32 of 46 copies

HYPERVELOCITY KILL MECHANISMS PROGRAM (U)

Advance Research Projects Agency
Order No. 149-60
Contract No. 3295(00)(X)

Aerothermal Phase

Quarterly Progress Report
For Period Ending
20 June 1963

D. E. Nestler, Technical Director

R. F. Welsh, Program Manager

"This document contains information affecting the national defense of the United States within the meaning of the Espionage Laws, Title 18, U.S.C., Sections 793 and 794. Its transmission or the revelation of its contents in any manner to an unauthorized person is prohibited by law."

General Electric Company
Re-entry Systems Department
Philadelphia 4, Pennsylvania

Reproduction of this report in whole or in part is permitted for any purpose by the United States Government.

H

LAN: 3964-46-1
4148-02-1

SUMMARY

Work continued in the areas of flight and ground tests designed to obtain basic data on internal heating phenomena of perforated re-entry vehicles.

The second NASA Wallops Island flight test was launched on 7 May 1963, and again resulted in successful telemetry of data throughout re-entry, with successful recovery of the model. Preliminary data are being analyzed.

The model for the internal heating tests of coupled and uncoupled flow was completed and delivered to Cornell Aeronautical Laboratory for testing in the Wave Superheater Facility. Tests will be conducted in July.

A program has been initiated to determine flow characteristics of various geometry orifices having supersonic tangential approach flow. A detailed description of the test objectives and concept is included. Tests are scheduled for AEDC Tunnel E-1 in October.

A checkout of the main subroutines of the IBM 7090 Internal Heating Computer Program has been completed. A complete checkout of the program will be conducted concurrent with parametric studies. Plans for additional modifications of the program are discussed.

The thermostructural investigations were resumed with studies of the Mark 3 vehicle. Emphasis is being placed on the stresses at the cone-cylinder juncture due to penetration of the conical portion.

During the past quarter, emphasis was placed on flight and ground tests designed to obtain basic data on internal heating phenomena of perforated re-entry vehicles. Thermostructural studies of structural failure modes were resumed. Descriptions of progress in each phase of the program are given below.

WALLOPS ISLAND FLIGHT PROGRAM

The second flight was launched on 7 May 1963, and again resulted in successful telemetry of data throughout re-entry, with successful recovery of the model. The second flight model contained an inlet orifice on the nose cap 60 degrees away from the stagnation point, plus two vent ports on the cone. Unexpectedly severe ablation occurred immediately downstream of the inlet orifice.

A review of preliminary results of beta flights was held at NASA Langley, followed by release of preliminary pressure and temperature data. Analysis of the data will be made in the coming quarter, including comparisons with Malta Rocket Exhaust results of identical models.

INTERNAL HEATING TESTS

The model for the internal heating tests of coupled and uncoupled flow was completed and delivered to Cornell Aeronautical Laboratory for testing in the Wave Superheater Facility. A description of the model and test conditions was given in Reference 1. The tests are now scheduled for late July, due to a delay in facility test schedule on other programs.

ORIFICE FLOW TESTS

Tests will be conducted in AEDC Tunnel E-1 to determine the flow characteristics of orifices having supersonic tangential approach flow. Flow rate, as well as velocity profiles and direction of the expanded jet, will be determined as functions of approach Mach number, orifice thickness-to-diameter ratio, and orifice pressure ratio. In addition, the effects of orifice diameter and obliquity on flow rate and jet direction will be determined for various orifice-to-thickness ratios at one approach Mach number, and the effects of orifice shape on flow rate and jet direction will be determined for one orifice thickness-to-diameter ratio at one approach Mach number.

The tests will be performed by mounting a box to the tunnel side wall at the orifice test section. Steady state flow rates will be established by evacuating the box by means of a vacuum pump, to the desired pressure ratios. The flow rate thru the orifice will be measured by a calibrated flow meter. The static pressure upstream and downstream of the orifice will be measured in order to permit correlation of the results in terms of a dimensionless flow coefficient. Pitot surveys of the expanded jet will be conducted within the box at several distances downstream of the orifice exit. Photographs (Schlieren or shadowgraph) of the expanded jet within the box will be obtained for each run. At the completion of each run, the vacuum pump will be shut down, and photographs will be taken of the flow pattern existing within the box with no box outflow. Boundary layer velocity profiles on the tunnel wall will be obtained upstream and downstream of the orifice.

The results will be analyzed to verify theoretical and empirical methods of computing flow rate, jet direction, and jet diffusion as functions of the independent variables. This information is needed to perform internal heating analyses of perforated re-entry vehicles.

A preliminary design of the model and instrumentation has been completed by AEDC personnel to assure model compatibility with the tunnel facility. The detailed design and manufacture of the model and associated instrumentation will be performed by GE/RSD.

A tentative test schedule has been set up with AEDC and the Air Force. Tunnel time in E-1 is anticipated to be four weeks, from 30 September to 25 October 1963, inclusive.

PARAMETRIC COMPUTATIONS

A checkout of the main subroutines of the IBM 7090 Internal Heating Program has been completed. A complete checkout of the program will be conducted concurrent with parametric studies on the C-1 Advanced Concept Target Vehicle. It is also planned to use the program to perform predictions of internal heating and pressure for the Wallops Island flight models.

In the present form, the program is set up to predict internal heating for uncoupled flow conditions, either vented or unvented. It is planned to modify the program to also accommodate coupled flow conditions based on the internal heating tests being conducted at the Cornell Aeronautical Laboratory. In addition, the program will be updated periodically to reflect advances in state-of-the-art of internal heating technology in the areas of orifice flow characteristics, jet diffusion, jet impingement heating, and wall jet heat transfer.

STRUCTURAL STUDIES

The thermostructural investigations were resumed with studies of the Mark 3 vehicle. The cone-cylinder forward cavity structure of this vehicle is being investigated, since this type of structure behaves differently than the conical shells previously studied. A penetration of the conical shell resulted in an equalization of internal and external pressure (assuming uncoupled flow) thus reducing the contribution of the mechanical loads to the failure mechanism. A penetration of the conical portion of the Mark 3 cone-cylinder structure results in a pressure equalization of the conical section and an outward acting pressure on the cylindrical section.

The stress level at the cone-cylinder juncture due to this differential pressure loading may be appreciable and thus cause failure at a higher altitude than that conservatively estimated using the melting temperature of the shell only. The actual determination of this effect is the immediate goal of this study.

The trajectory shown in the previous HKM Annual Report, Reference 2, is being used. The specific vehicle geometry and weight distribution were obtained from past RSD documents. Using this trajectory, vehicle geometry and aerodynamic characteristics, structural loads were calculated for the vehicle at various times along the re-entry path. The resulting stresses are being calculated at the cone-cylinder juncture using the above loads and influence coefficients computed for this specific vehicle geometry.

REFERENCES

1. GE/RSD, "Hypervelocity Kill Mechanisms Program", Semi-annual Progress Report for Period Ending March 1963, GE Document 63SD555 (Secret)
2. GE/RSD, "Hypervelocity Kill Mechanisms Program," Annual Progress Report for Period Ending 20 September 1962, GE/RSD Document 62SD806 (Secret)

HYPERVELOCITY KILL MECHANISMS PROGRAM

ARPA Order 149-60

Aerothermal Phase

Quarterly Progress Report
For Period Ending
20 June 1963

Coleman duP. Donaldson
K. Evan Gray
Roger D. Sullivan
Richard S. Snedeker

Aeronautical Research Associates of Princeton, Inc.
50 Washington Road, Princeton, New Jersey

SUMMARY

The efforts at ARAP in the several areas of responsibility with which it is concerned are reviewed briefly. These areas include over-all management and coordination tasks as well as theoretical and experimental work on jet decay, jet impingement, wall jet problems, and coupled flow phenomena. Certain problems which will receive close attention in the coming year are mentioned.

MANAGEMENT AND COORDINATION

Among the usual liaison and interpretive duties required under this portion of the program, ARAP has been involved, during the past quarter, in several projects which should be mentioned herein.

1. A meeting was held on April 22, 1963, at ARAP including representatives of ARAP, ONR, AVCO, and General Electric to discuss the current status of the efforts of the various participants in the Aerothermal Phase and to outline future plans. Recent results achieved by these groups in their various experimental and theoretical efforts were presented and discussed.

2. A paper covering the various technical problems of aerothermal kill mechanisms was presented at the Sixth Symposium on Hypervelocity Impact in Cleveland on May 2, 1963.

3. A preliminary study was performed on the feasibility of using foam materials for the protection of vehicle interiors against aerothermal effects. A memorandum was prepared which summarized briefly the pertinent current information on such foams.

Further study of the problems of flow coupling and buoyancy has been made and plans have been formulated for additional investigations of these problems during the coming year.

The experimental study of coupled flows under way at ARAP has been described in previous Progress Reports.

JET IMPINGEMENT AND WALL JET STUDIES

Theoretical

A theoretical study has been undertaken in an attempt to develop a theory for the incompressible turbulent radial wall jet which will agree with present experimental information and which may be extended to the case of compressible flow. This study has been undertaken so as to have a rational theory for the distribution of heat transfer in the region adjacent to an impinging jet.

Experimental

A detailed discussion of the jet impingement experimental program was presented in the previous Progress Report. Subsequent to that report, the tests for normal impingement on all four models have been completed. The data are now in the process of reduction and no additional conclusions will be presented at this time. Because of the obvious importance of local shock structure in an underexpanded free jet, a detailed survey was made with the flat plate model in the region of supersonic impingement. The results of this series of tests should make possible a more meaningful interpretation of all the impingement data taken under similar underexpanded conditions for the other models.

A program to gather data under conditions of oblique impingement is now in progress.

DISTRIBUTION

	<u>No. of Copies</u>
Director Advanced Research Projects Agency Washington, D.C. Attn: Mr. J.E. Blower	4
Director Ballistic Research Laboratories Aberdeen Proving Ground Aberdeen, Maryland Attn: Dr. F. Allison	1
Director U.S. Naval Research Laboratory Washington 25, D.C. Attn: Mr. W.W. Atkins	3
General Electric Company 3198 Chestnut Street Philadelphia, Penna. Attn: Mr. D. Nestler	1
AVCO Corporation 201 Lowell Street Wilmington, Mass. Attn: Dr. T. Mix	1
Commander DET 4, (ASQWR) ASD, AFSC Eglin AFB, Florida Attn: Mr. D. Davis	1
Aeronautical Research Associates of Princeton 50 Washington Road Princeton, N.J. Attn: Dr. C. Donaldson	1